AN ABSTRACT OF THE THESIS OF

Jason B. Brandes for the dual degree of Master of Science in Water Resources Science and Environmental Engineering presented on June 12, 2017.

Title: The Vadose Zone as a Hyporheic Carbon Source: A Look at Temporal Trends in Hyporheic Zone pCO_2

Abstract Approved:

Roy Haggerty Lewis Semprini

Stream chemistry studies conducted in the forested Watershed 1 of the HJ Andrews Experimental Forest show a contribution of CO_2 from the hyporheic zone. Hyporheic CO_2 concentrations, measured as pCO_2, have a seasonal trend as well as a responsiveness to storm events. Concentrations are highest at the end of the dry season (~14,000 µatm) and lowest during the wet season (~6,000 µatm). Hyporheic pCO_2 has been observed in a well to respond to winter storm events with a sudden decrease followed by a sharp increase in pCO_2. The increase in pCO_2 exceeds pre-storm levels, suggesting an additional contribution of pCO_2 into the hyporheic zone. Concentrations gradually return to pre-storm levels as stream discharge decreases. I hypothesize that surplus CO_2 is flushed into the hyporheic zone from the overlying soil (vadose zone) during storm events. I tested the hypothesis by monitoring soil gas (pCO_2) at equilibrium with soil water, temperature, water table height, and soil moisture content at various depths throughout the m^2 soil column of our study site. I modeled well F2 dissolved CO_2 concentrations to compare to observed F2 dissolved CO_2 concentrations to determine the contribution of CO_2 from the vadose zone to hyporheic flow during storm events. The findings from the study suggest that the

connectivity from the vadose zone to the hyporheic zone is seasonal, dissolved CO_2 contribution from the vadose zone to the hyporheic zone occurs when the soil is sufficiently saturated to enable complete percolation from the vadose zone to the hyporheic zone, our study column can be described as “dry”, “transitional”, and “wet”, and prior to complete saturation the system is a complex network with unidentified boundaries.

The Vadose Zone as a Hyporheic Carbon Source: A Look at Temporal Trends in Hyporheic Zone pCO_2

by

Jason B. Brandes

A THESIS

Submitted to

Oregon State University

in partial fulfillment of
the requirements for the
degree of

Master of Science

Presented June 12, 2017

Commencement June 2018

Master of Science thesis of Jason B. Brandes presented on June 12, 2017.

APPROVED:

Co-major Professor, representing Water Resources Science

Co-major Professor representing Environmental Engineering

Director of Water Resources Graduate Program

Head of the School of Chemical, Biological and Environmental Engineering

---

Dean of the Graduate School

I understand that my thesis will become part of the permanent collection of Oregon State University libraries. My signature below authorizes release of my thesis to any reader upon request

---

Jason B. Brandes, Author

ACKNOWLEDGEMENTS

I would like to thank Dr. Roy Haggerty and Dr. Mary Santelmann first and foremost for providing me with the opportunity to attend graduate school. I would also like to thank the National Science Foundation for the project funding. Additional acknowledgement goes to Dr. Steve Wondzell, Dr. Mary Dragila; the folks at the OSUCAL lab especially Gloria Ambrowiak; Dr. Tyler Radnieki for his encouragement; the wonderful staff at the H.J. Andrews; and lastly the Stream Carbon Team for humor and scientific adventure.

CONTRIBUTION OF AUTHORS

I would like to emphasize my gratitude to the following: Dr. Roy Haggerty for the countless hours of planning and discussing this project; Dr. Jonathan Istok and Dr. Semprini for helping me design the model used in this analysis; Robert Pennington for his thoughts, suggestions, and encouragement; Dr. John Selker for his thoughts and encouragement; Dr. Brian Wood for his thoughts, suggestions, and encouragement; Dr. Mary Santelmann for borrowed equipment; Dr. John Dilles for the rock sample analysis; Ceili Shannon for her survey help; Dr. Julia Jones and Fred Swanson for their "folk knowledge" about H.J. Andrews; and Dr. Steve Wondzell for his voluminous work in Watershed 1. I wish to extend a sincere thank you to all for their time and patience.

TABLE OF CONTENTS

			Page
1.	Abstract	……	01
2.	Introduction	……	02
3.	Methods and Experimental Design	……..……	14
	3.1	Equipment Bundle……....	16
	3.2	Equipment Testing…….	21
	3.3	Equipment Deployment…….....	22
	3.4	Soil Sample Lab Analysis……..	24
	3.5	MODEL……..	26
	3.5.1	Contributing Area Analysis……	30
	3.5.2	Models and Equations……	31
	3.6	Assumptions……...	35
4.	Results		
	4.1	Raw Data Observations……..	36
	4.1.1	Well F2 CO_2 Concentration…….....	40
	4.1.2	Shallow and Deep CO_2 Concentrations……..	40
	4.2	van Genuchten K(θ) and Soil Hydrology……...	41
	4.3	Changes in Pressure Head and Vadose Zone Model Activation……...	41
	4.4	Storm 2……...	43
	4.5	Storm 4…….....	47
	4.6	Storm 6……..……..	49
	4.7	Model Sensitivity and Verification……	51

TABLE OF CONTENTS (Continued)

			Page
5.	Discussion	……	54
	5.1	Dry Period…….....	55
	5.2	Transitional Period…….	56
	5.3	Wet Period…….	56
	5.4	Contributing Area vs. Correlation and Connectivity…….	56
	5.5	Seasonality, Changes in Pressure Head, Hysteresis, Mixing, Contributing Area……...	58
	5.6	MODEL Sensitivity and Verification…….	56
	5.7	Further Study……..	59
	5.7.1	End Member Mixing Analysis……..……..	60
6.	Summary	……	61
7.	Conclusions	……	64
8.	Bibliography	……	65
	Appendix A	Nomenclature…….	68
	Appendix B	Methods additional materials…….	70
	Appendix C	Results additional materials..…….	75
	Appendix D	Photo gallery……..……	86

LIST OF FIGURES

Figure		Page
1.	Stream and hyporheic pCO_2, discharge, temperature, and precipitation data…..	08
2.	H.J. Andrews Experimental Forest with Watershed 1 denoted as WS1……..	10
3.	LIDAR image of well field……..	12
4.	Box model of study column…….	15
5.	In-situ probes, well F2, and piezometer in the study column……...	17
6.	Preparation steps for GMM 220 probe deployment…….	19
7.	Soil moisture probe housing procedure……	20
8.	Process for prepared CO_2 probe deployment……...	24
9.	Soil sample moisture release curve……..	25
10.	Model percolation requirements ……..	27
11.	Soil moisture with depth over time ……..……...	27
12.	Pressure head (P) and hydraulic conductivity (K) vs soil moisture (ϑ)……...	28
13.	Model surface area planes……	29
14.	Flow lines from extending contributing areas…….	31
15.	van Genuchten-Mualem models vs pressure head (P)…….	32
16.	van Genuchten-Mualem models correlation plot…….	33
17.	Storms of interest during wet season……	39
18.	Storms 2 (A), 4 (B), 6 (C) change in pressure head with stage height…….	42

LIST OF FIGURES (Continued)

Figure	Page
19. Vadose zone hydrological model activation for storms 2, 4 and 6 (A-C respectively)……	43
20. Storm 2 with a contributing area of 1 m^2……..……	45
21. *E* coefficients vs contributing areas (m^2) from values in Table 2 ……...	46
22. Storm 4 with a contributing area of 5 m^2……..……...	48
23. *E* coefficients vs contributing area ……...……...	48
24. Storm 6 with a contributing area of 65 m^2……...	50
25. *E* coefficients vs contributing area ……...……...	51
26. Fitting coefficient sensitivity analysis……...……..	53
27. Contributing area change with time…….	55

LIST OF TABLES

Table		Page
1.	Model input values ……...……..…….	44
2.	Storm 2 *E* coefficients with increasing contributing areas …….	46
3.	Model input values……..	47
4.	Storm 4 *E* coefficients with increasing contributing areas …….	49
5.	Model input values ……...	50
6.	Storm 6 *E* coefficients with increasing contributing areas …….	51
7.	α sensitivity analysis range of values ……..	85
8.	*m* sensitivity analysis range of values.…….	85

LIST OF APPENDIX FIGURES

Figure	Page
28. . Full year plot 10/2015 - 10/2016……	69
29. Survey data used to determine $\frac{\partial h}{\partial Z}$ for hyporheic K_{Sat} …….	70
30. Pressure transducer model with observed data……	71
31. Pressure transducer model vs stage height plot……...	71
32. Storm 2 with a contributing area of 100 m^2…….	75
33. Storm 2 with a contributing area of 500 m^2…….	75
34. Storm 2 with a contributing area of 1000 m^2……	76
35. Storm 2 with a contributing area of 2000 m^2……	76
36. Storm 2 with a contributing area of 5000 m^2……	77
37. Storm 4 with a contributing area of 1 m^2……..…….	77
38. Storm 4 with a contributing area of 10 m^2……	78
39. Storm 4 with a contributing area of 25 m^2……	78
40. Storm 4 with a contributing area of 50 m^2……	79
41. Storm 6 with a contributing area of 1 m^2…….	79
42. Storm 6 with a contributing area of 25 m^2……	80
43. Storm 6 with a contributing area of 50 m^2……	80
44. Storm 6 with a contributing area of 85 m^2……	81

LIST OF APPENDIX FIGURES (Continued)

Figure Page

45. Storm 6 with a contributing area of 95 m^2…… 81

46. Storm 6 with a contributing area of 150 m^2……. 82

47. Storm 6 with a contributing area of 500 m^2…….. 82

48. Model response to a change in α ……...…….. 83

49. Model results using OSUCAL K_{Sat}…….. 84

50. Model results using "Loam" K_{Sat} [*Dingman*, 2008]……. 84

51. Change in model discharge with K_{sat} increase……. 85

52. View of WS1 from above confluence looking northwest…… 86

53. View of study site from above ……...…….. 87

54. View of well field from bridge ……..…….. 87

55. View of study column……... 88

56. Two additional views of study column and experimental rain simulator…… 88

57. Vaisala probe in PVC casing…… 89

58. Deployment of PVC encased probe……. 89

59. Deployed Vaisala probe in outer PVC casing…….. 89

60. Campbell datalogger……. 89

LIST OF APPENDIX FIGURES (Continued)

Figure	Page
61. View of rain collector from study column……...	91
62. View of rain collector from trail……...	92
63. Rain collector close-up…….	92

1. Abstract:

Stream chemistry studies conducted in the forested Watershed 1 of the HJ Andrews Experimental Forest show a contribution of CO_2 from the hyporheic zone. Generally, hyporheic CO_2 concentrations, measured as pCO_2, have a seasonal trend as well as a responsiveness to storm events. Concentrations are highest at the end of the dry season (~14,000 µatm) and lowest during the wet season (~6,000 µatm). Hyporheic pCO_2 has been observed in a well to respond to winter storm events with a sudden decrease followed by a sharp increase in pCO_2. The increase in pCO_2 exceeds pre-storm levels, suggesting an additional contribution of pCO_2 into the hyporheic zone. Concentrations gradually return to pre-storm levels as stream discharge decreases. I hypothesize that surplus CO_2 is flushed into the hyporheic zone from the overlying soil (vadose zone) during storm events. I tested the hypothesis by monitoring soil gas (pCO_2) at equilibrium with soil water, temperature, water table height, and soil moisture content at various depths throughout the m^2 soil column of our study site. I modeled well F2 dissolved CO_2 concentrations to compare to observed F2 dissolved CO_2 concentrations to determine the contribution of CO_2 from the vadose zone to hyporheic flow during storm events. The findings from the study suggest that the connectivity from the vadose zone to the hyporheic zone is seasonal, dissolved CO_2 contribution from the vadose zone to the hyporheic zone occurs when the soil is sufficiently saturated to enable complete percolation from the vadose zone to the hyporheic zone, our study column can be described as “dry”, “transitional”, and “wet”, and prior to complete saturation the system is a complex network with unidentified boundaries.

2. Introduction:

Imbalances in the global carbon budget have been a topic of study for several years. Research has focused on the various pathways to determine their individual contributions. Portions of the terrestrial carbon budget are transported to the world's oceans through rivers and streams, evaded to the atmosphere, or stored in living and decaying organic matter in soils. An early model of rivers and streams viewed them collectively as an inert "conduit" through which carbon was transported from the terrestrial watersheds to the oceans [*Cole et al*., 2007]. Carbon budget models that used the conduit view may have underestimated the amount of carbon being released into the atmosphere and overestimated the amount of carbon being stored [*Cole et al*., 2007; *Hope et al*., 2001]. A current view of rivers and streams is one in which the system is not a conduit but rather a network of processes that serve as carbon sinks and sources [*Cole et al*., 2007]. This more inclusive understanding of rivers and streams may enable researchers to provide a more accurate estimate of terrestrial carbon transport as ongoing research describes the connectivity of the soil–streambed-stream-atmosphere continuum.

Terrestrial waters supersaturated with dissolved CO_2 with respect to atmospheric concentrations are the driving force for surface water CO_2 efflux into the atmosphere [*Hope et al*., 2001]. Cole et al. suggest that of the total 1.9 Petagrams (Pg) C/yr of terrestrial carbon going into rivers and streams, 0.75 Pg C/yr is being evaded from stream surfaces, while 0.23 Pg C/yr is being stored in sediment. The remaining 0.9 Pg C/yr is being delivered to the ocean in streams and rivers [*Cole et al*., 2007]. Other studies report annual stream CO_2 efflux of 1.8 Pg C, and an export of 0.8-1.2 Pg C [*Raymond et al*., 2013; *Butman et al*., 2014; *Richey et al*., 2002]. According to Raymond, 70% of stream CO_2 efflux occurs on stream and river surfaces which make up roughly 20% of the global terrestrial surface area [*Raymond et al*., 2013]. Collectively,

riparian zones, hyporheic zones, flood plains, groundwater and the streams are a source of CO_2 to the atmosphere, and these numbers emphasize the impact of streams as part of the global carbon budget.

Streams serve as a collection of lateral carbon inputs from groundwater, surface runoff water, hyporheic water and instream carbon transformations [*Cole et al.*, 2007]. The lateral input of carbon into streams occurs from the hillslopes to the riparian corridor adjacent to streams in a watershed. The instream CO_2 is a combination of newly produced CO_2 within the stream and riparian soils, and old CO_2 that has entered the system from deep sources [*Rinehart et al*., 2015]. A study found that, spatially, instream dissolved CO_2 concentrations vary as function of: hydrologic connectivity to riparian soils, watershed topography, organic matter abundance, geology, and riparian soil type [*Hope et al*., 2001].

The soils in riparian corridors adjacent to streams are the location of many biogeochemical processes that can uptake carbon into cell mass, accumulate carbon particles during adsorption, produce CO_2 through cellular and root respiration, and conversion of carbon species during chemical reactions with local lithology [*Cole et al*., 2007]. One study showed that riparian soils can be a greater sink for carbon than vegetation at a ratio of 4:1 [*Jarvis et al*., 2007], which suggests that they may have a great impact on the global carbon budget. But what biogeochemical or physical processes in the soil are responsible for the release or storage of carbon?

Riparian soils can be spatially heterogenous and thus the production, transport, and transformation of carbon can be spatially heterogenous. Organic matter that serves as a source of carbon for diverse microbial communities can be highly variable in abundance, availability, and location in the soil. Soil water content and connectivity is an important facilitator of nutrient

transport. The hydrologic connectivity within a soil network can be highly variable which can result in isolated carbon sources that do not contribute to system wide movement of respiration and respiration products [*Rinehart et al*., 2015]. Soils that drain readily have been found to have high rates of soil respiration and vertical evasion [*Hope et al.*, 2001]. Riparian soils can be highly variable with respect to soil respiration and respiration products transport depending on soil moisture [*Tang et al*., 2005]. Vertical percolation of surface water can connect different soil layers within a column, and one study cites that in addition to percolation, subsurface water flow in forested hillslope soil can also follow macropores such as from decayed roots or worms [*Harr*, 1977]. The aforementioned soil is from a hillslope soil study but I suggest that the principles remain true for riparian soils.

Seasonality is a major factor that can influence soil respiration. Precipitation events following seasonal trends alter soil moisture and temperature. Temperature and soil moisture are the primary contributing factors to CO_2 production in some soils [*Jarvis et al*., 2007]. Termed the "Birch effect", the periodic wetting and drying of soils can result in short lived but significant pulses of CO_2 evasion from soil surfaces as a product of a microbial population increase and subsequent heterotrophic respiration [*Birch*, 1964; *Jarvis et al*., 2007]. This study was conducted in a Mediterranean climate, which has distinct dry and wet seasonal characteristics.

Currently there are several hypotheses as to how this occurs. One in particular suggests that following a period of drought, a pulse of moisture into the soil promotes increased decomposition of organic material due to microbial population increase [*Jarvis et al*., 2007]. Soils that maintain a low level of moisture did not tend to experience these bursts of activity such as soils found in temperate forests [*Birch*, 1964], however, Birch effects have been observed in these types of soils following a long period of drought [*Birch*, 1964; *Jarvis et al*., 2007]. Other

Birch effect findings include: the amount of organic carbon in the soil can determine the amount of CO_2 emitted from the surface, the dryer the soil the greater the Birch effect can be, and organic soil carbon processing declines with each successive wetting event [*Jarvis et al*., 2007]. In addition to changes in soil moisture, temperature changes can affect respiration rates, gas efflux, and gas solubility. Warmer temperatures enhance respiration rates and gas efflux, while cooler temperatures decrease respiration rates and subsequent efflux and increase gas solubility [*Tang et al*., 2005; *Dosch*, 2014].

Following the findings described by *Birch* [1964], studies conducted by *Tang et al*. [2005] and *Johnson et al*. [1994] show that soil columns do not have a constant concentration of CO_2 (mg L^{-1}), but rather a gradient that is influenced by root and microbial CO_2 production, soil moisture and temperature. Generally, CO_2 concentrations increase with depth creating an overall vertical concentration gradient that exits at the soil surface under constant diffusivity. *Tang et al*., [2005] found that short term precipitation events can create regions of high respiration closer to the surface thereby creating a reverse concentration gradient. They also observed that increased soil moisture resulted in increased soil respiration up to a point, beyond which, increased soil moisture began to have negative effects on soil respiration. When soil moisture was too high the pathways by which the gas could travel to the surface would become blocked by water molecules. When soil moisture was held constant, their model produced results indicating that increasing temperature led to an increase in respiration [*Tang et al*., 2005]. In agreement with this, *Johnson et al*. [1994] found that the decreased temperatures of the fall and winter months may reduce microbial respiration. *Johnson et al*. [1994] also found that surface CO_2 efflux showed a higher correlation with soil moisture than with soil temperature. These two studies illustrate the relationships between soil pCO_2 soil conditions.

The hyporheic zone is defined as a network of relatively short flow-paths that leave from and return to the stream in hyporheic exchange. These flow paths are located in the saturated zone of the riparian soils adjacent to streams [*Kasahara and Wondzell et al*. 2003]. The stream is a source of dissolved organic carbon (DOC) and dissolved inorganic carbon (DIC) which enter the soil along these hyporheic flow paths becoming a source of energy for soil microbial respiration. A study found that extended residence time through longer hyporheic flow paths can convert higher amounts of DOC into DIC through increased contact with microbial communities. In addition, higher water velocities passing through these hyporheic flow paths have resulted in more DOC processing [*Rinehart et al*., 2015]. The overall effect is the stream being supplied with respiration products thereby increasing the dissolved CO_2 concentration in the main channel.

Low order streams may have an important contributing role in the global carbon budget. The global surface area of rivers and streams is thought to be roughly 20% of total land surface. This surface area represents a massive site for gas exchange and therefore the source for a considerable input of CO_2 into the atmosphere [*Downing*, 2012]. This estimate does not include times of flooding or drought. *Butman & Raymond* [2011] found that first order streams comprised 20% of the total stream surface area possibly indicating higher CO_2 concentrations with lower order stream sources. Smaller streams that are typically lower order tend to have high surface area and high surface efflux of CO_2 due to gas exchange which is influenced by turbulent flow [*Downing*, 2012]. Precipitation events can also impact stream CO_2 evasion as flushing and stream surface area increase [*Butman & Raymond*, 2011; *Raymond et al*., 2013]. *Butman and Raymond* [2011], report that streams of lower Strahler order have higher CO_2 concentrations than streams of higher Strahler order. The CO_2 evasion from the stream air interface can decrease the

channel CO_2 concentration moving downstream. Studies show an average CO_2 drop of 128 µatm with each increase in stream order and distance from headwaters [*Butman & Raymond*, 2011; *Dosch*, 2014].

A study conducted by *Argerich et al*. [2016] in Watershed 1 (WS1) of the H. J. Andrews found that stream CO_2 evasion increases followed precipitation events as well as a pattern of lowest stream pCO_2 concentrations during the wet season. DOC concentrations were observed to increase with the onset of the wet season followed by a decrease in DOC concentration suggesting a flushing mechanism of accumulated DOC in riparian soils during the dry months. Conversely, DIC concentrations are high in the dry season and low during the wet season suggesting dilution by low DIC containing water [*Argerich et al*., 2016]. Another study conducted by *Dosch* [2014] in WS1 found that during periods of low flow the discharge is lower resulting in elevated instream concentrations of pCO_2. Likewise, during the wet season when there is higher discharge, evasion is abundant resulting in lower instream concentrations of pCO_2 [*Dosch*, 2014].

According to the previously discussed research we can expect seasonal trends in the stream/ hyporheic zone/ vadose zone/ atmospheric continuum. Seasonal rain events will bring changes to soil moisture content and soil temperature, which may result in changes in respiration, gas transport, and rates of CO_2 evasion from the soil surface. Periodic rain events may result in the development of reverse concentration gradients as CO_2 concentrations increase near the soil surface from respiration hotspots. We can expect changes in pCO_2 in soils that have roots as the changing seasons will result in diel fluctuations associated with photosynthesis that change as deciduous leaf coverage declines during the cooler months or increases during the warmer months. We can also expect vertical CO_2 evasion interrupted by periods of lateral pCO_2 transport

when soils are saturated. Seasonality will also affect stream and hyporheic pCO_2. The model of the WS1 hyporheic network described by *Dosch* [2014] suggested that periods of low flow will result in higher stream pCO_2 from hyporheic exchange, and periods of high discharge will result in higher rates of stream surface CO_2 efflux. Lastly, we may see a distinct data signature that may be linked to precipitation events [Figure 1]. During the rising limb of the hydrograph the hyporheic pCO_2 steeply drops followed by a steep increase in pCO_2 that extends beyond pre-hydrograph rise levels. The pCO_2 peak gradually falls to roughly pre-storm pCO_2 levels during the falling limb of the discharge line. This same pCO_2 response to precipitation events was observed in a continuous measurement stream study conducted by *Johnson et al*. [2009]. It is the origin of this storm response that we are interested in understanding.

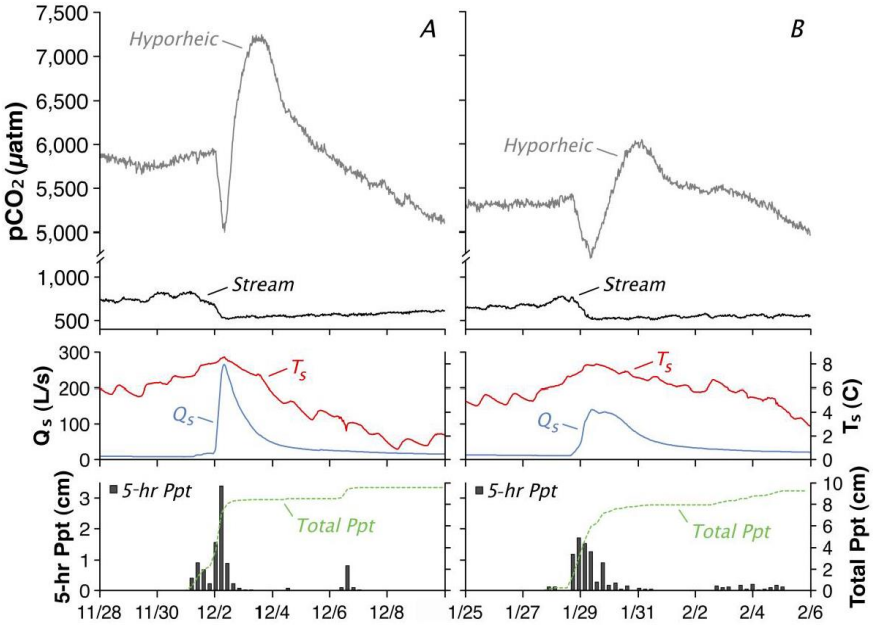

Figure 1. Stream and hyporheic pCO_2, discharge, temperature, and precipitation data. The figure shows stream and hyporheic CO_2 concentrations (µatm), stream temperature (^oC), steam flow (L s^{-1}), and precipitation (cm) [*Dosch*, 2014].

My study site is located in the lower portion of WS1 in the H. J. Andrews Experimental Forest (HJA) in the Western Cascades of western Oregon in the United States of America (44^{o} 10'N, 122^{o} 15'W)[Figure 2]. The climate of the HJA is defined by mild winters and long dry summers. Roughly 80% of the annual precipitation falls between October and April as long duration frontal storms. Snow accumulates at the higher elevations of the forest and can result in spring runoff during melting, and can also accumulate for short periods of time in the lower portions of WS1 [*Harr*, 1977]. The regional geology is of volcanic origin and is comprised of a mixture of pyroclastic flow products, lava flows and dikes. The current geologic and topographic state at the Andrews is one that has resulted from a legacy of volcanism, glaciation, weathering, and hydrothermal activity. Most of WS1 (outlined bottom left corner of HJA in Figure 2) is underlain by a mixture of volcaniclastic rocks though a portion of the upper reaches of WS1 are underlain by basaltic flows. There has not been any carbonate bedrock found in WS1 which eliminates CO_2 production from carbonate rock weathering. WS1 has historically experienced both deep-seated and shallow mass movements which occurred at the upper elevations of the watershed. The cause for these mass movements may be the abundant presence of clays in the volcaniclastic soils [*Swanson & James*, 1975]. WS1 is steeply inclined with forested slopes and a narrow floodplain that serves as the riparian corridor for a small 2nd order stream at an elevation interval of approximately 410 m to 1630 m [*Argerich et al*., 2016; *Dosch*, 2014]. The riparian valley floor is characterized by debris jams, logs, and sediment steps created by these obstructions [*Wondzell*, 2006]. The steep topography is the result of a volcanic history and water incision [*Swanson & James*, 1975]. The slopes are forested with predominantly Douglas fir (*Pseudotsuga menziesii*) and the valley floor is predominantly red alder (*Alnus rubra*) and vine maple (*Acer circinatum*) [*Wondzell et al*., 2010]. The watershed was clear cut in 1962 and 1966.

Following the 1966 harvest, WS1 was burned and later replanted with Douglas fir saplings [*Argerich et al*., 2016].

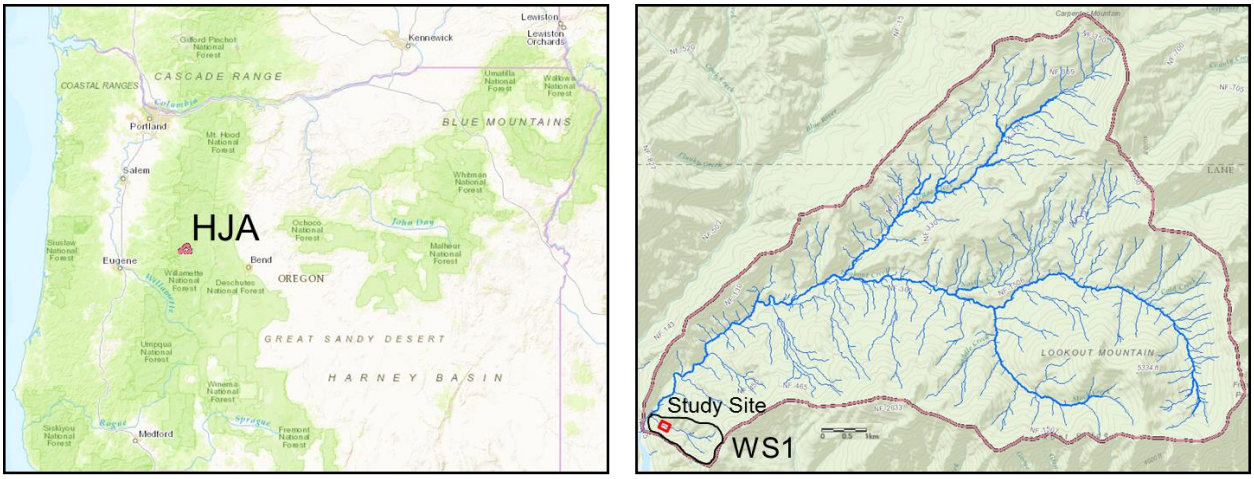

Figure 2. H.J. Andrews Experimental Forest with Watershed 1 denoted as WS1 [HJA website].

The soil of the valley floor is a highly heterogenous mix of sand, clay, cobble, boulders, and wood due to past debris flows. There have not been any recorded debris flows since installation of a stream gauge in the 1950s [*Wondzell*, 2006]. A soil study conducted in 1962 in the upper slopes of WS1 categorized the soil found there as "Limberlost" which is comprised of breccias and volcanic tuffs and is classified as a Regosol [*Dyrness*, 1969]. Regosols in general are well drained, colluvium forms soils found on steep slopes and ridges. These types of soils are considered to have particle sizes that are "fine to loamy" with a clay content of 18 – 35%. The Limberlost soil has been broken into two categories when defining total porosity and percent pore-space. The categories are "topsoil", and "subsoil." The values for total porosity for topsoil and subsoil are approximately 68 and 63% respectively [*Dyrness*, 1969]. Given the mass-

movement history of WS1, it may be that some of the finer components of the highly mixed, poorly sorted soil column for this study may be comprised of Limberlost soil. This is an important point because the porosity of the shallow soil observed in this study may be comparable to the Limberlost topsoil porosity. However; it should be noted that mass movement materials can resort themselves and finer sediments can be lost [*Wondzell*, 2006]. Within the riparian subsoil is a network of hyporheic paths with a down-valley gradient 1.4 times greater than the cross-valley gradient that are the result of hyporheic exchange due to downwelling and upwelling [*Wondzell*, 2006]. Some of these hyporheic paths have been found to be long and running parallel to the stream with median residence times of 17 hours [*Wondzell*, 2006].

The study area [Figure 3] [Figures 59-60, Appendix D] lies in the valley floor which has a roughly 13% incline to the southeast and is on average roughly 14 m wide at an elevation of roughly 500 m and receives drainage from an approximately 100-ha catchment [*Wondzell et al*., 2010; *Swanson & James*, 1975]. The unsaturated (vadose zone) of the soil column in the well network of WS1 are on average 70 cm thick while the average riparian soil depth is 2 m thick [*Wondzell et al*., 2010]. The valley floor is topographically complex with logs, and point bars [Figure 3].

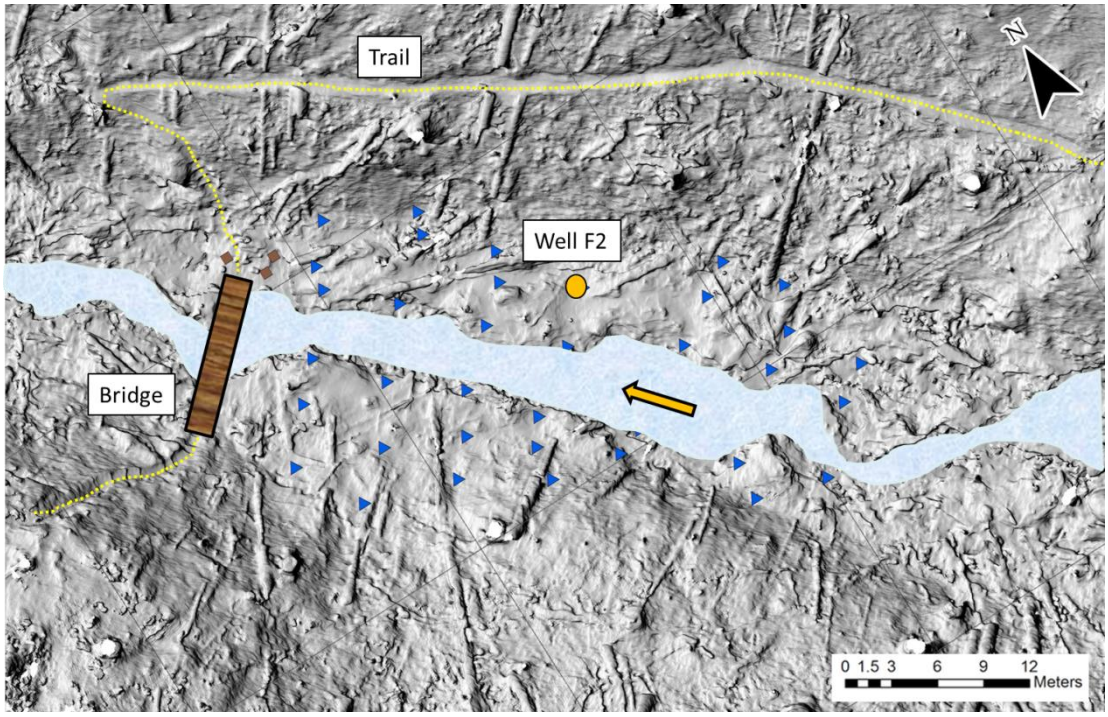

Figure 3. LIDAR image of well field. Well F2 shown as a yellow dot, trail is shown as a dotted yellow line, direction of flow going east to west shown as a yellow arrow, and wells in well field shown as blue triangles.

The study focused on well F2 in [Figure 3] and the other wells are denoted as blue triangles. The study site has a network of 37 wells installed into the valley floor and piezometers installed directly in the stream channel. The wells are 2-inch (5.08 cm) stainless steel pipes that are screened at the bottom and have removable caps at the tops. They range from 1 – 2 meters in length, and vary in ground penetration. The wells are arranged in six parallel transects perpendicular to the stream from valley edge to valley edge.

Research conducted by *Corson-Rikert* [2014] showed that DOC decreased along hyporheic flow paths with longer residence times, as DIC increased along the same flow paths. This is thought to be the result of microbial respiration along these hyporheic flow paths

[*Corson-Rikert*, 2014]. Additionally, the observed DIC concentration increase was found to be higher than could have been produced by stream sourced DOC metabolism. The author suggests that there may be DOC and DIC being contributed to the hyporheic channels by the vadose zone through a periodic flushing mechanism [*Corson-Rikert*, 2014].

The system hydrologic connectivity is seasonal, and the highly permeable adjacent slopes enable storm precipitation to quickly move through the surface into the subsurface and into the main channel creating a "flashy" stream [*Harr*, 1977; *Dyrness*, 1969]. However; during times of low flow, the hydrologic connectivity between the steep hillslopes and the valley floor were minimal in WS1suggesting that the hyporheic water table was sustained primarily by hyporheic exchange with the stream and not the surrounding slopes [*Wondzell et al.*, 2010].

Through this series of connections and observations a few questions have become clear. Is there CO_2 flushing from overlying riparian soils into hyporheic flow paths? Is there a seasonal component to the pCO_2 flushing? Are we seeing a Birch effect at the beginning of the wet season? I will address these questions by monitoring a study site within the riparian corridor of WS1 for approximately one year in order assess the temporal patterns and fluxes of pCO_2 that originate in the soil layers (vadose zone) overlying the hyporheic zone. I hypothesize that the vadose zone is a source of pCO_2 for the hyporheic zone and that seasonal rainstorms are the catalyst for the pCO_2 transport. I will use the data collected during larger storm events to test the hypothesis by creating a model that will predict dissolved CO_2 concentrations in well F2 that I can statistically compare to observed well F2 dissolved CO_2 concentrations. My goal is to use the model to predict dissolved CO_2 concentrations that are identical to observed dissolved CO_2 concentrations in well F2. I posit that identical or similar dissolved CO_2 concentrations indicate contribution to the hyporheic zone from the vadose zone.

3. Methods and Experimental Design:

I developed a model to examine pCO_2 concentrations and initiate transport from the vadose zone to the hyporheic zone at the appropriate times. I first developed a hydraulic model using physical soil and groundwater flow properties that I used to transport the dissolved CO_2 from the vadose zone into the hyporheic zone. Next I used a mixing model to combine the horizontal hyporheic zone flux with the vertical vadose zone flux into a resultant theoretic well F2 pCO_2 concentration. I then compared the predicted dissolved CO_2 concentrations at well F2 with the observed dissolved CO_2 concentrations using statistical analyses. I used the collected data as the model inputs. I collected soil moisture, pCO_2 concentrations, and temperature at multiple depths as well as water-table elevation in the study column. I focused on six storm events during the wet season using stream stage height data as an indicator for precipitation events. Stage data were calculated using a weir that has been in use in WS1 for several decades. The stage height data was provided by the HJA website.

I focused on a smaller portion of the wet season because I wanted to be able to look closely at the soil CO_2 variability with depth before and after saturation. The time of the investigation can be divided into three different periods based on the observed soil hydrology: "dry"; "transitional"; and "wet". These dry, transitional, and wet periods are associated with storms 2, 4, and 6 respectively.

I focused on: vadose zone (A), deep soil zone between the vadose and hyporheic zones (B), hyporheic zone (C) [Figure 4]. The white triangles in figures 4 and 5 depict the water table. There is not a clearly defined saturated zone due to capillary rise above the water table.

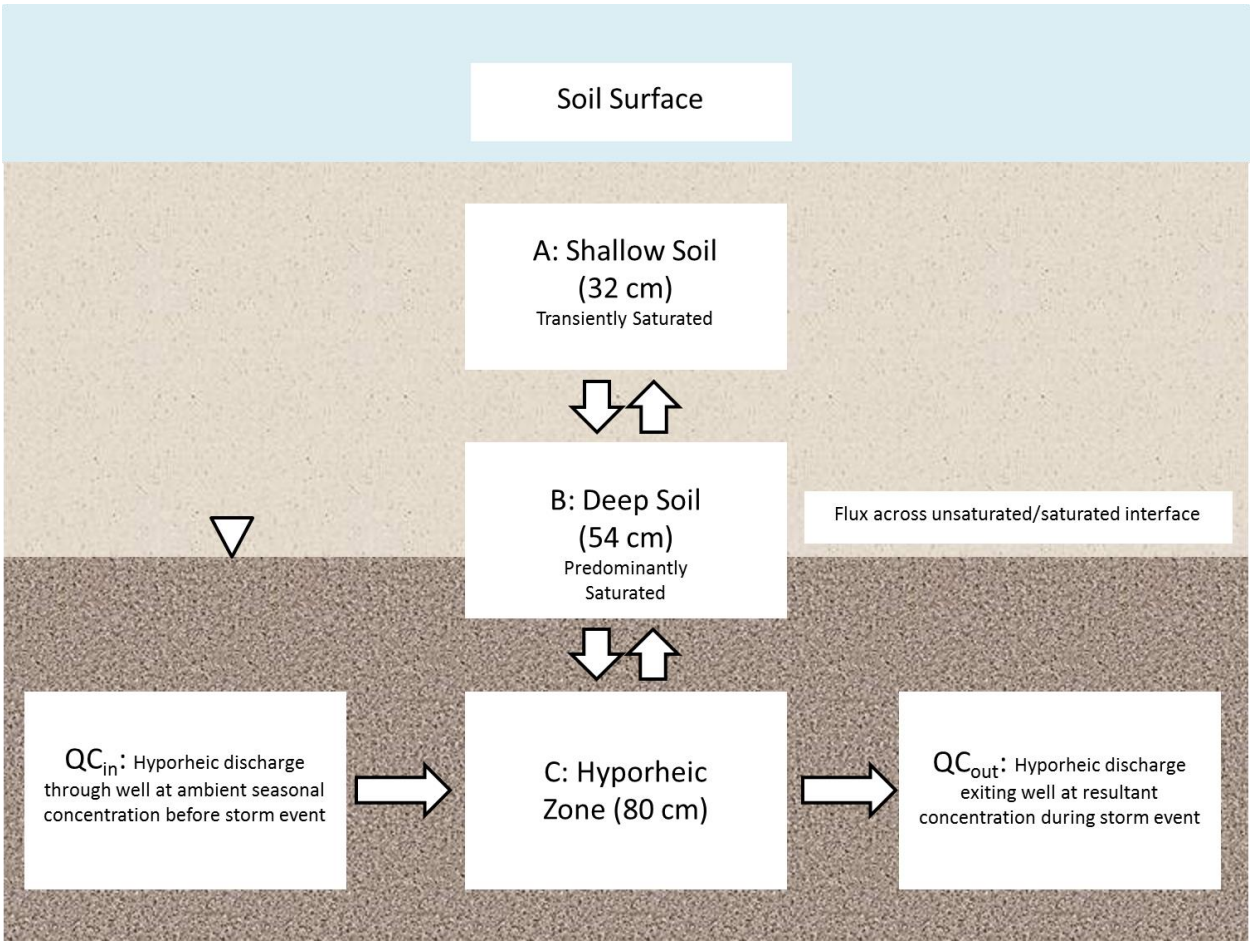

Figure 4. Box model of study column. The hyporheic zone portion of the box model receives continuous flow through it with a changing concentration of dissolved CO_2. The vadose and deep soil zones have changing concentrations and movement of CO_2 in both gaseous and dissolved phases as indicated by the arrows pointing up and down.

It should be noted that my study focused only on the analysis of dissolved CO_2 transport in the vadose, deep soil and hyporheic zones of the study site soil profile. A more complete analysis would include quantifying the gas transport within the column following the methods described by *Tang et al.* [2005]. I decided to focus on the dissolved CO_2 transport because I want to predict the contribution from the vadose zone to the hyporheic zone.

3.1 – Equipment Bundle

I instrumented my study plot to monitor soil CO_2 in both the saturated and unsaturated zones in slightly less than a cubic meter of soil centered at well F2 [Figure 5] ~3 meters from the stream at my research site [Figures 52-57, Appendix D]. I focused the instruments around well F2 to observe the conditions in the soil that facilitate pCO_2 contribution to the hyporheic water flowing through well F2. The purpose of the instrumentation "bundle" was to be able to collect continuous data at 10 minute intervals over the course of a year in order to build a data base that can describe some of the soil column's physical and chemical characteristics at various depths. The bundle consists of four Vaisala GMM220 CO_2 probes, two Stevens Water Monitoring Systems Inc. HYDRA II soil moisture probes, a pressure transducer, twelve Tidbit temperature loggers, and a Campbell CR 200x DataLogger. The pressure transducer was deployed in a PVC pipe well adjacent to well F2, and the Tidbit temperature loggers were deployed at depths ~25 cm and ~54 cm in multiple locations close to well F2.

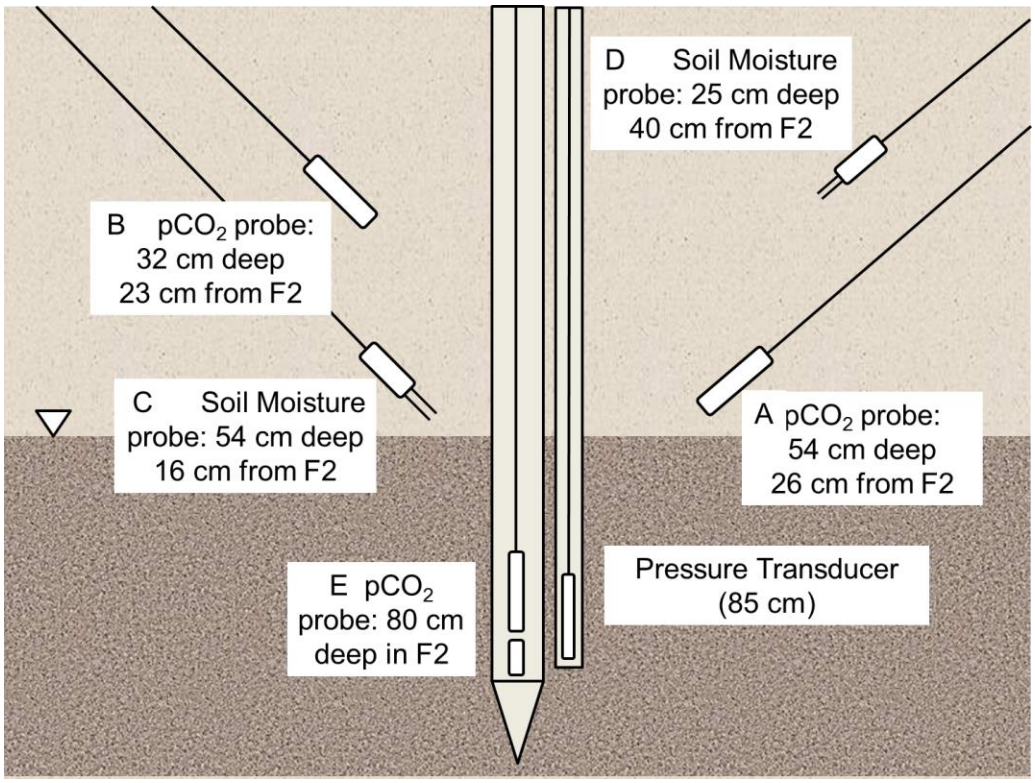

Figure 5. In-situ probes, well F2, and piezometer in the study column. Figure not to scale. Figure illustrates the approximate depths and distances from well F2 of each probe not including the 12 x Tidbit temperature loggers. The figure shows the orientations, depths and distances of the instruments with respect to well F2.

The Vaisala GMM220 CO_2 probes use infrared gas analyzers (IRGAs) housed in a durable plastic case with a cord that extends to a circuit board. The GMM220 can be deployed *in situ* in a variety of environments. The internal technology consists of a single beam dual wavelength non-dispersive infrared (NDIR) light source and a silicon based sensor cap (Carbocap). NDIR technology works using CO_2 absorbance which indicates concentration. Additionally, the single-beam dual-wavelength technology is reported by Vaisala to not have issues with data drift. The CO_2 gas circulates across the IRGA gas bench generating a mole

fraction value (ppm, µatm) that is transmitted through the *ex situ* components to a data-logger. The partial pressure units given by the probe (µatm) needed to be converted to dissolved CO_2 concentrations (mg/L) for the mixing model [*Johnson et al*., 2009].

The case of the probe is approximately 15 cm long and 2 cm in diameter. The GM220 probe is designed for deployment in rugged and humid environments but the IRGA gas bench cannot come into contact with water. Following the methods described in *Johnson et al*. [2009] I encased the probes in a gas-permeable/water-impermeable polytetrafluoroethylene (PTFE) membrane which allows the dissolved CO_2 to diffuse from solution across the membrane to be analyzed by the probe. The ends of the PTFE tube were clasped together using plastic zip ties and finally sealed using several coats of Liquid Tape™. The probes were then housed in PVC casings with ample holes to allow ease of flow across the membrane, and then finally a layer of metal screen was wrapped around the portion of pipe containing the holes in order to protect from rocks and sand [Figure 6].

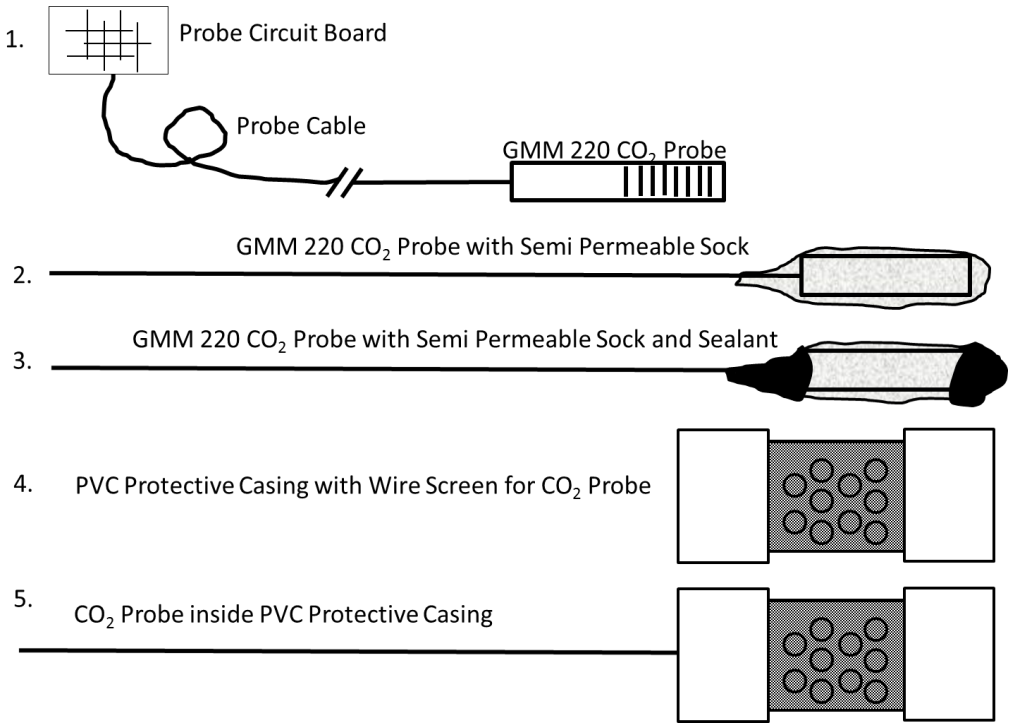

Figure 6. Preparation steps for GMM 220 probe deployment. Figure not to scale.

The Hydra II soil moisture probes uses a reflected electromagnetic radio wave to determine the dielectric permittivity in soils. This method uses the Stevens Water Monitoring Systems Inc. patented algorithms to convert the dielectric permittivity into soil electrical conductivity and soil moisture. The soil moisture measurements are presented as volumetric water fraction (θ, $m^3\ m^{-3}$, wfv), and saturation values are soil dependent. I was not permitted to conduct any destructive soil sampling within the test zone, so my best estimate was to use the default factory "loam" setting. The manufacturer's manual also supports using the "loam" setting based on the table of calibration settings and soil type. All probe wiring, care, and testing procedures follow the Stevens Water Monitoring Systems Inc. Hydra II operating manual.

The probe is comprised of a hard plastic head unit with a flat stainless steel base from which four stainless steel tines extend. The tines are 45 mm in length and 3 mm thick and the space between them is the "sensing volume." The base plate is 25 mm in diameter. The probe electronics are housed in the plastic head unit with a durable cable running out of the top to an external data-logger. The probes were seated in a PVC coupler with a hole drilled to allow the cable to run through. The coupler was glued to a smaller diameter PVC pipe with the cable running inside and out the top [Figure 7]. The purpose of the pipe was to protect the cable and allow for minimal disturbance of the soil upon deployment. An important point to consider when deploying the probes was to make sure that the base plate had good contact with the soil. Another reason to seat the probe into the PVC structure was to allow us to gently but firmly thrust the probe into the soil.

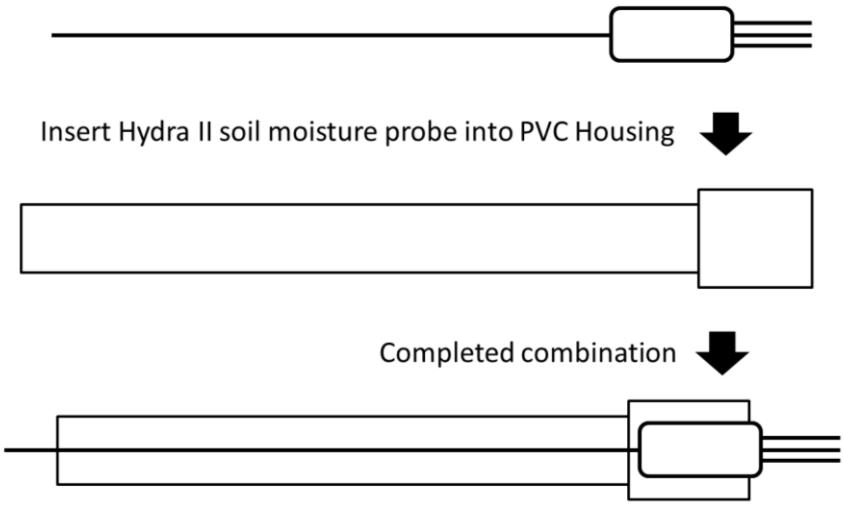

Figure 7. Soil moisture probe housing procedure. Figure not to scale.

3.2 – Equipment Testing

The CO_2 probes were calibrated before deployment by insertion into an airtight chamber with gas of a known CO_2 concentration (1010 ppm). The probes were given approximately 1 hour to equilibrate with the gas in the chamber while concentration readings were monitored. Each probe had a variance of ~60 ppm (before conversion to µatm) which converts to 0.1 mg/L at 20 ^oC.

The Hydra II soil moisture probes were benched tested using a variety of soils with varying moisture content. The soils were taken from a steep gradient stream in a forested catchment adjacent to Alsea highway 34 approximately 0.76 miles west of Botkin road southwest of Philomath Oregon with similar vegetative assemblage to field site i.e., alders, maples, and Douglas firs. The samples were taken from a hillslope location, and 3 floodplain locations. The samples were weighed and each probe was inserted for a moisture reading. The samples were then oven dried at low heat (130 ^oF) for 72 hours. The samples were then weighed and each probe was inserted again for a dry soil moisture reading. Comparison of the values recorded when the soil samples were both wet and dry revealed that the probes were recording similar soil moisture values with higher correlation ($R^2 = 0.99$) in the wet soils. I assumed that the quality assurance process at the manufacturer was sufficient for acquiring accurate reliable soil moisture readings, but I wanted to make sure that each probe was taking similar readings. Additionally, the dielectric permittivity was tested following manufacturer procedures described in the instrument manual provided by Stevens Water Monitoring Systems Inc.

The pressure transducer was tested by submerging probe into a bucket of water and comparing true depth to calculated depth. The TIDBIT temperature probes were tested before deployment by exposing them to hot water and cold water at known temperatures.

All probes were observed in the lab for functionality upon being hardwired to the CR200x secured within the protective Campbell field case before being taken to field site for deployment. All probes except the temperature probes were wired directly into the data-logger. The temperature probes data were downloaded using a TIDBIT interface on a lab computer terminal.

3.3 – Equipment Deployment

I wanted to minimize soil disturbance at the site, so care was taken when installing our instruments into the subsurface. I wanted to collect data that was as representative of natural undisturbed conditions as possible. To accomplish this, I used 2" diameter metal spikes to punch holes into the soil to create paths that we could use to install all equipment *in situ*. There was no digging and/or removing of soil material at the site.

Well F2 was installed near the location of a previous well [*Kasahara and Wondzell*, 2003] that was removed from the well field in WS1. I used a 2-inch diameter stainless steel pipe that came with an 8-inch (20.32 cm) perforated and screened section at the bottom. The overall length of the well was ~1.2 m with ~0.87 m below the ground surface, not including the nose cone. The well was installed, developed and monitored for clean consistent flow prior to this study. Well development was performed by filling it with water and pushing the water down through the well screen using a pipe with a gasket fixed to the end that provided a tight fit to the inside of the well. The purpose for this was to flush away the fine soil surrounding the well screen to prevent screen clogging. This method was repeated several times until clean water flowed into the well. The pressure transducer was installed into a piezometer made of 1.5-inch (3.81 cm) PVC pipe ~8 cm from well F2 to a depth of ~84 cm. The soil moisture and CO_2 probes were installed at roughly 45 degree angles to prevent preferential flow paths of surface water that

may have occurred had the PVC pipes been installed vertically [Figure 5]. I wanted to prevent preferential flow paths to avoid short circuiting of surface water directly to the probes, thereby giving a false sense of the time it takes water to percolate through the soil. The important aspect was to facilitate natural percolation of surface water to reach the probes to get a reading was more representative of soil water properties at a specific depth. The Tidbit probes were similarly deployed using a pipe to create a shaft through which the probes could be lowered to depths of 32 and 54 cm. The shafts were then filled in to prevent the probes from recording surface air temperatures.

The CO_2 probes were deployed at various depths below surface (0, 32, 54, 90 cm). The soil moisture probes were installed at 25 and 54 cm depth. Probe deployment depths were calculated using lengths of pipe submerged below the surface and distances from well F2. The purpose for these depths was to be able to monitor surface, unsaturated, and saturated soil depths. The CO_2 probes were deployed in a series of pipes that can fit into each other [Figure 8] giving me the ability to deploy and extract the probes with little to no soil disturbance. The probes were isolated from surface air using electricians putty and therefore captured CO_2 concentrations at the terminus of the pipes.

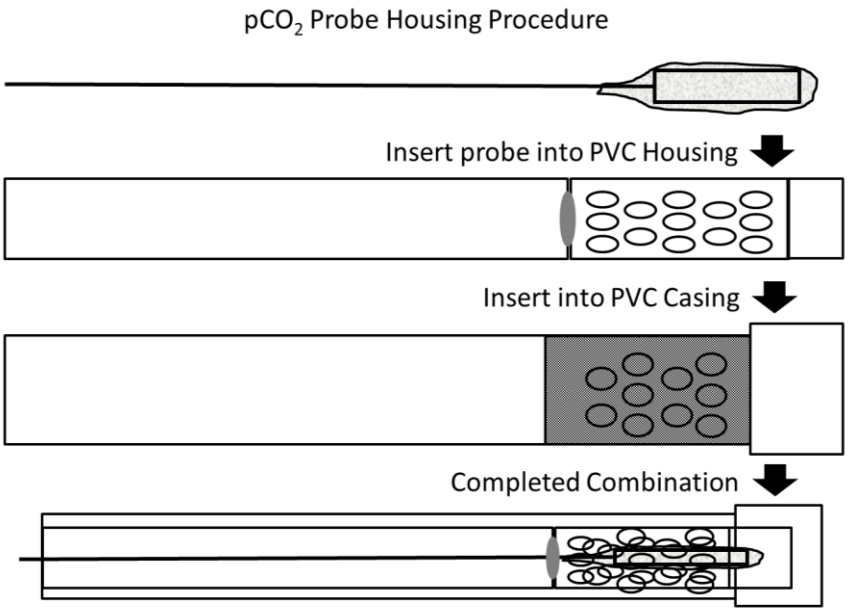

Figure 8. Process for prepared CO_2 probe deployment. Figure not to scale.

3.4 – Soil Sample Lab Analysis

We needed a soil moisture release curve and a saturated hydraulic conductivity (K_{sat}) to be able to perform the calculations for the hydraulic model. We were not able to extract a soil sample directly from the study site, so a location downstream of the study site was chosen as a sample collection point. The soil where the sample was taken needed to be as similar to soil conditions at my study site as possible. The intact core sample was taken ~2 meters from the stream at a location with similar surface conditions i.e., organic material mixed in with the top layer of sand, gravel, and some clay overlaying gravel, cobble, and sand. We assumed that this soil sample is representative of the soil at our study site and the subsequent calculated coefficients can be used to model water flow in the soil column. This dual layer description is

based on personal observations when installing wells throughout the well field, and instruments into my study column.

The analyses were conducted in the Oregon State University Central Analytical Laboratory (OSUCAL). A Decagon HYPROP was used to generate the soil moisture release curve following the Decagon HYPROP protocols manual [Figure 9].

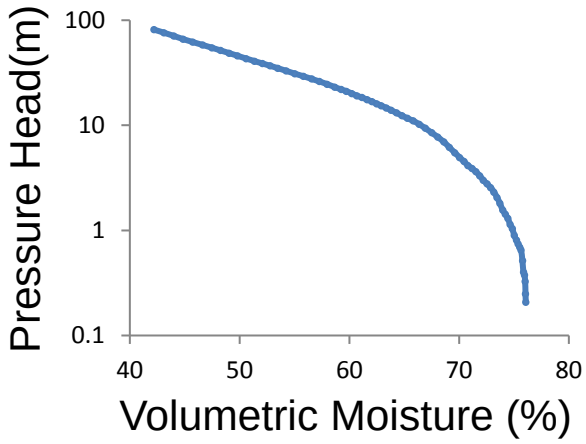

Figure 9. Soil sample moisture release curve. Volumetric moisture describes volume of water over the volume of soil (%).

The hyporheic zone Ksat value was determined by performing a slug test [Appendix B] [*Bouwer*, 1969]. The vadose zone K_{sat} value was calculated following OSUCAL standard operating procedures for constant head (1) and falling head methods (2). The constant head method uses flux (Q), column length (L), cross sectional area (A) and head (h). The falling head method uses L, A, change in head (a), time (t), initial head ($h1$), final head ($h2$), and the coefficient 2.3.

$$K = \frac{QL}{Ah} \quad (1)$$

$$K = \left[\frac{2.3aL}{At}\right] ln\left(\frac{h1}{h2}\right) \quad (2)$$

The K_{sat} results for the constant head and falling head methods were 1.5 cm/day, and 1.7 cm/day respectively which are small when compared to literature K_{sat} values for loam soils (3.2×10^{-3} – 6.95×10^{-4} cm s^{-1}) [*Selker et al*., 1999; *Dingman*, 2008].

3.5 – MODEL

The vadose zone flows used in the model were based on soil moisture (Θ) changes during storms. The model engages only at times when there is infiltration from the vadose zone into the hyporheic zone which occurs only when there is a positive total head (h) gradient resulting from soil saturation in the vadose zone. Positive h occurs when the highly negative pressure head (P) value rises towards 0 cm allowing the elevation head (z) to become the driving force for soil fluid movement. The study column experiences complete percolation only when saturated [Figure 10]. This is because when the soil is not saturated the pressure head (P) values are highly negative and the subsequent total head (h) values are highly negative as well. When negative total head values are utilized in equation (10) the resulting flow (Q) has a positive value which means that flow is moving upwards. The hydraulic conductivity (K) in the vadose zone also changes with soil moisture. The following figures are conceptual cartoons depicting: changes in Θ with depth, z and changing time t [Figure 11]; and changes in K and P with Θ [Figure 12].

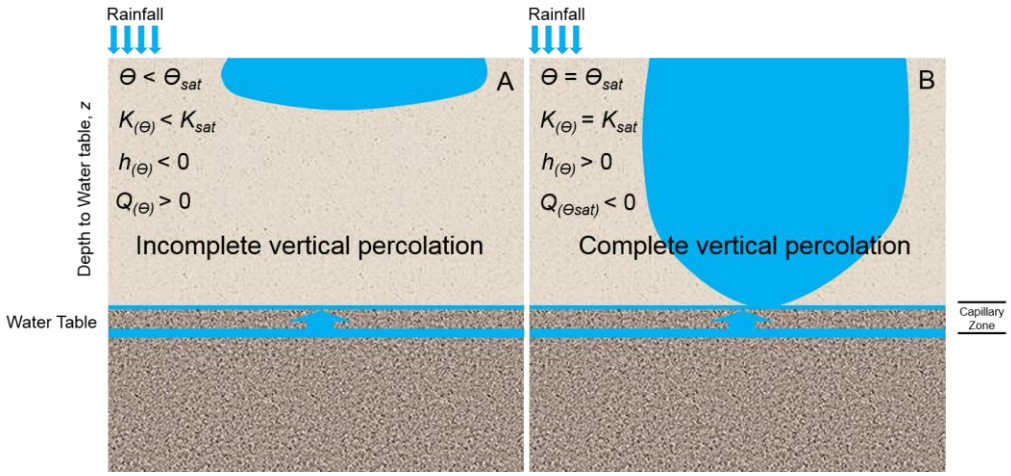

Figure 10. Model percolation requirements. Original conceptual diagram based on concepts described by *Schwartz and Zhang* [2003] and *Selker* [1999]. Diagram represents model soil column.

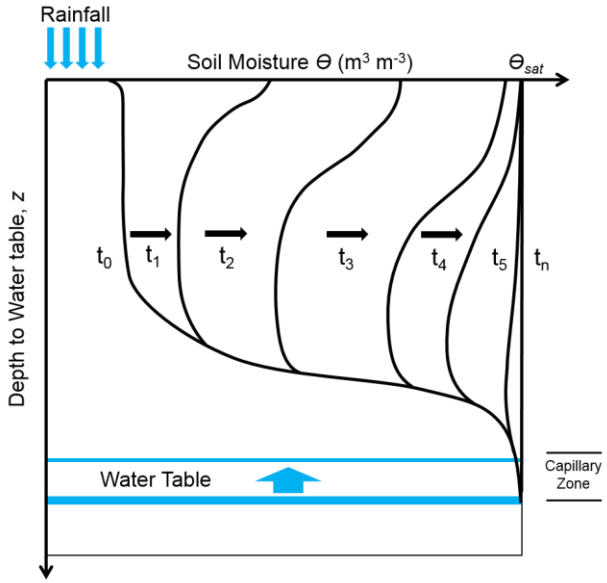

Figure 11. Soil moisture with depth over time. Modified version of a figure presented by the website [http://echo2.epfl.ch/VICAIRE/mod_3/chapt_4/main.htm], and based on concepts discussed by *Schwartz and Zhang* [2003].

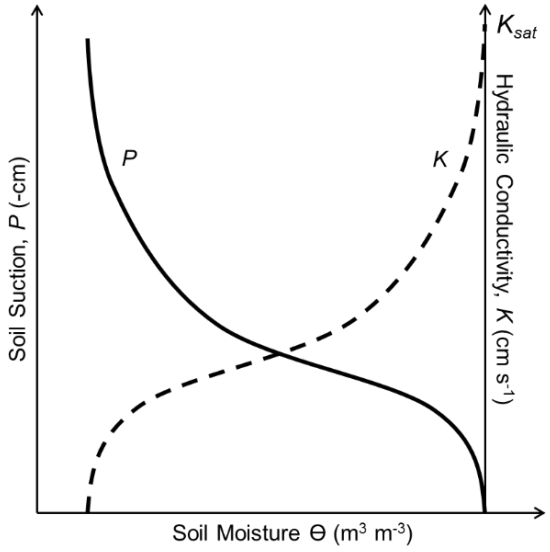

Figure 12. Pressure head (P) and hydraulic conductivity (K) vs soil moisture (ϑ). Modified version of a plot and concepts presented by *Schwartz and Zhang* [2003].

The fluxes from the vadose zone flowing into the hyporheic zone results in change in dissolved CO_2 concentrations and discharge with time. Additionally, the flux flowing through the hyporheic zone results in changes in dissolved CO_2 concentrations and discharge with time. The mixing model [Figure 13] will use both fluxes to predict a dissolved CO_2 concentration. The K_{sat} in the vadose zone is an order of magnitude smaller than the K_{sat} in the hyporheic zone and is the limiting factor for vertical flow and subsequent flux into the hyporheic zone. To make CO_2 predictions, we assumed that the hyporheic CO_2 concentration is constant and the model volume is completely mixed with the flux from the vadose zone. The mixing model component of the model simulates fluxes in a 0.4 m^3 soil block. The horizontal area through which the vertical flux passes is assumed to be 1.0 m^2. The vertical area through which the horizontal flux from the hyporheic flow passes is assumed to be 0.4 m^2. The hyporheic concentration (C_1) is a value that

is fixed to the pre-storm concentration because I wanted it to represent the hyporheic concentration before any potential flushing of CO_2 from the vadose zone into the hyporheic zone occurs. The hyporheic discharge (Q_1) changes with stage height during storm event.

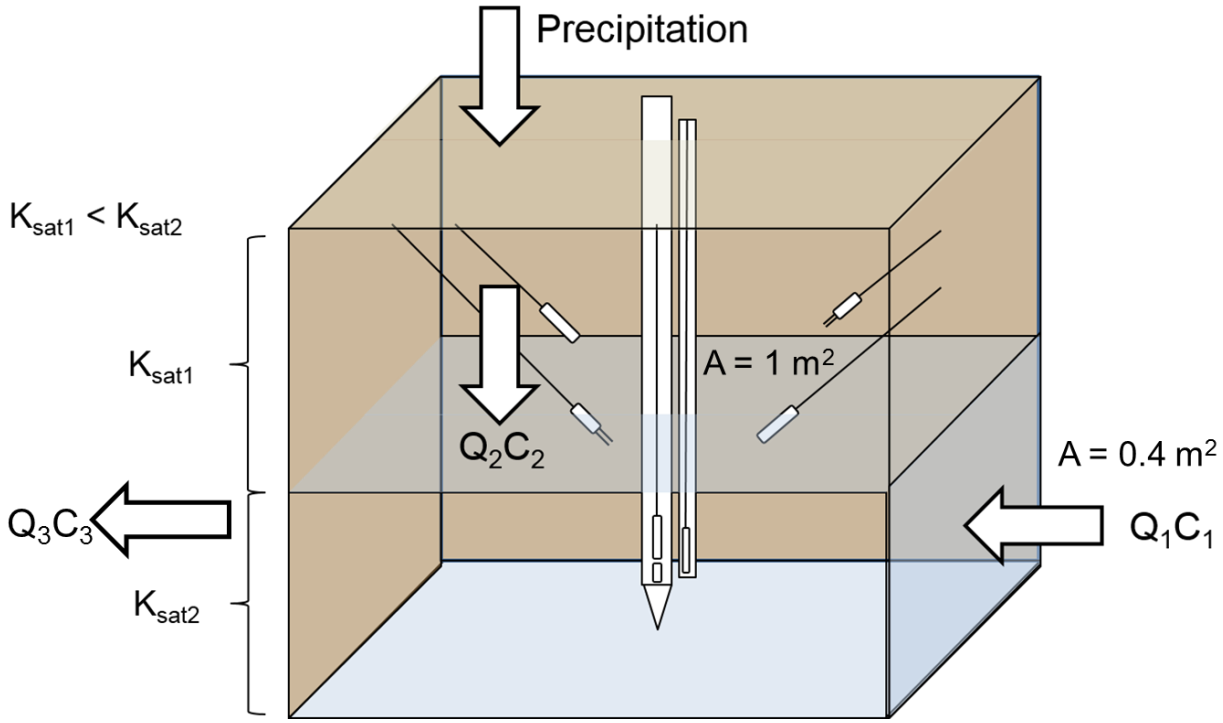

Figure 13. Model surface area planes. Figure not to scale. The objects in the center of the cube represent the instrument cluster as depicted in Figure 5. Flux from the vadose zone is labeled Q_2C_2 and flux through the hyporheic zone is labeled Q_1C_1. The vadose zone saturated hydraulic conductivity is labeled K_{sat1}, and the hyporheic zone saturated hydraulic conductivity is labeled K_{sat2}. Resultant discharge is labeled Q_3, and predicted CO_2 (mg/L) is labeled C_3.

I chose the areas to use in the model as initial values to verify that the model was functioning correctly. I acknowledge that both the vertical and horizontal contributing areas to the water flowing through the model hyporheic mixing zone may change with storm intensity

according to findings cited by *Wondzell* [2006]. As previously stated I chose to design the model with a 1 m^2 surface area centered on well F2 to model the soil around the well. I chose to use 0.4 m^2 as the hyporheic zone height because I did not know the depth of the hyporheic zone to use as the lower boundary, and I was uncertain about the depth of the upper boundary of the hyporheic zone. Additionally, I assumed that the lower soil moisture probe and CO_2 probe were both in the capillary fringe of the hyporheic zone as opposed to being within main body of the hyporheic zone. I assumed this based on soil moisture observations and CO_2 concentrations where the soil moisture for the deep probe was at saturation but the CO_2 concentrations for the deep CO_2 probe were at levels that were similar to the shallow CO_2 probe.

3.5.1 – Contributing Area Analysis

I estimated the contributing area parameter when conducting the analysis by changing the vadose zone input area and comparing the predicted results with the observed results. I wish to investigate if increasing vadose zone soil wetness results in vadose to hyporheic connectivity with decreasing distance from observation point. If there is vadose zone CO_2 contribution to the hyporheic zone, I want to know if there is a seasonal change in the area required for CO_2 contribution from the vadose zone to the hyporheic zone. I suggest that during storm events within the dry season there may be many small contributions of dissolved CO_2 from the vadose zone to the hyporheic zone spread out over a large vadose zone area. Alternatively, I suggest that during storms within the wet season the vadose zone soil is wet enough to contribute dissolved CO_2 to the hyporheic zone through percolation pathways spread out over a much smaller area due to soil column connectivity. I believe that the result for this wet season connectivity will be similar CO_2 concentrations at various depths within the study column.

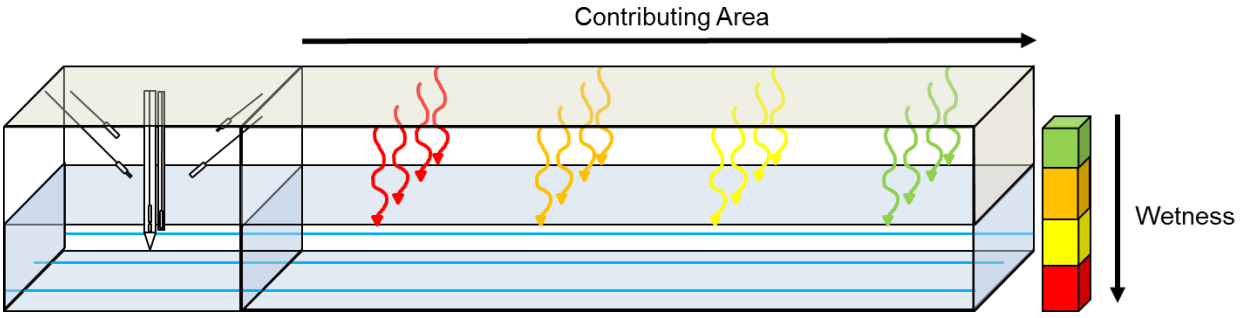

Figure 14. Flow lines from extending contributing areas. This is a cartoon of this concept where the different colored lines represent different locations upstream of the study plot and therefore a changing area of contribution. The blue lines represent the constant hyporheic flow through the plot [Figure 14]. It should be noted that flow through unsaturated media is generally vertical as flow in the hyporheic zone is generally horizontal. The curvature of the unsaturated flow lines in the figure is not representative of true unsaturated flow paths.

3.5.2 - Models and Equations

I used the soil moisture release curve and the relationship between pressure head (cm) and soil moisture (%) developed by van Genuchten and Mualem [1980] to determine the coefficients α and n [Figure 15].I used the pressure head values in the following equation (3) and changed α and n values until I achieved fitting curves between the two sides of the following equation where: Θ represents soil moisture value (wfv); Θ_r represents residual soil moisture (wfv); Θ_s represents saturated soil moisture (wfv); P is pressure head (cm); α relates to the inverse air entry pressure (cm^{-1}); and n represents the soil pore size distribution [*Mualem*, 1976; *Schaap*, 2000; *van Genuchten*, 1980]. The Θ_r and Θ_s are assumed values taken from observed soil moisture data. m is calculated using (4). Range of values in Appendix A.

$$\frac{(\theta - \theta_r)}{(\theta_s - \theta_r)} = \left[\frac{1}{1+(\alpha P)^n}\right]^m \quad (3)$$

$$m = 1 - 1/n \quad (4)$$

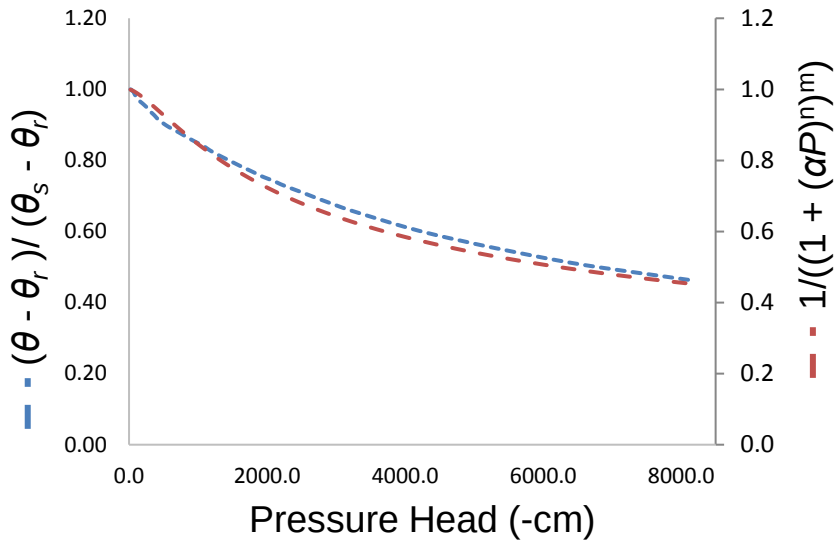

Figure 15. van Genuchten-Mualem models vs pressure head (*P*).

Following this I determined the closeness of the van Genuchten/Mualem relative saturation model based on soil moisture and the van Genuchten/Mualem relative saturation model based on α and n coefficients and achieved an R^2 value of 0.995. Based on this graphic analysis I determined the coefficients $\alpha = 8.5\ x\ 10^{-4}\ cm^{-1}$ and $n = 1.4$ that were used in my hydraulic model calculations [Figure 16].

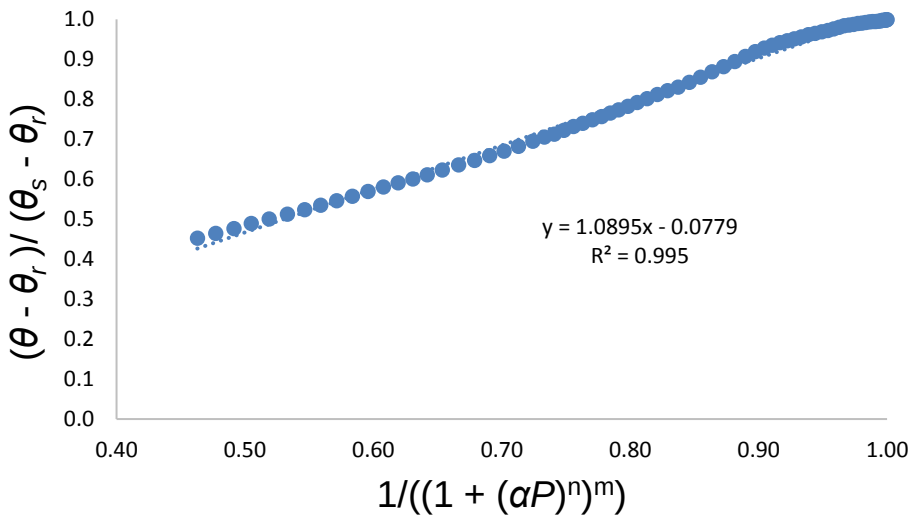

Figure 16. van Genuchten-Mualem models correlation plot.

I was then able to make hydraulic conductivity (*K*) calculations in the unsaturated zone based on soil moisture using the following equation (5) from [*Selker et al*., 1999], where K_{sat} represents the saturated hydraulic conductivity of the shallow soil layer. I used the K_{sat} determined by the OSUCAL (1.85×10^{-5} cm/s = ~1.6 cm/day).

$$K(\Theta) = K_{sat}\left(\frac{\theta - \theta r}{\theta s - \theta r}\right)^{0.5}\left\{1 - \left[1 - \left(\frac{\theta - \theta r}{\theta s - \theta r}\right)^{\frac{1}{m}}\right]^{m}\right\}^{2} \quad (5)$$

The pressure head (*P*) calculation in equation (6) is based on the van Genuchten equation (3). The purpose for this calculation is to determine the total head (*h*) value to be used in the discharge calculation.

$$P = \frac{\left(\left(\frac{\theta s - \theta r}{\theta - \theta r}\right)^{\frac{1}{m}} - 1\right)^{\frac{1}{n}}}{\alpha} \quad (6)$$

The Q_1 ($m^3\ s^{-1}$) values are connected to the stage height in the following equation (7) using: well F2 hyporheic K_{Sat}; observed stage height data labeled *Stage* (cm); pressure transducer model values labeled *PT Model* (cm); and fitting coefficient (C_f). Coefficient C_f represents the hyporheic contributing area and distance from stream, equation (8). These values are uncertain and are subsequently included within the fitting coefficient. The fitting coefficient was determined using the Solver function in Microsoft Excel© by solving for the minimum value of equation (9). I used the sum of the squared difference between model and observed dissolved CO_2 values because the model uses the hyporheic discharge but with unknown hyporheic flow path length and cross sectional area. The fitting coefficient allowed me to find the best fit for model dissolved CO_2 values to the observed dissolved CO_2 values at a given vadose zone contributing area.

$$Q = -K_{SAT}(Stage - PT\ Model)C_f \tag{7}$$

$$C_f = \frac{A}{\partial z} \tag{8}$$

$$\sum(Model\ CO_2 - Obs\ CO_2)^2 \tag{9}$$

Lastly, I used a mixing equation (10) to calculate the resultant CO_2 concentration in mg/L (C_3) in well F2. The components are: observed hyporheic concentration of CO_2 at a fixed pre-storm value in mg/L entering mixing volume (C_1), upstream hyporheic flow in m^3/s entering mixing volume (Q_1); CO_2 concentration in mg/L entering mixing volume from vadose zone (C_2); and flow in m^3/s entering mixing volume from vadose zone (Q_2) [*Schnoor*, 1996]. The Q values for the vadose zone and hyporheic zone differ depending on their respective constraints. The hyporheic Q_1 is limited by stage height whereas the vadose Q_2 is limited by soil moisture.

$$C_3 = \frac{C_1Q_1 + C_2Q_2}{Q_1 + Q_2} \tag{10}$$

We tested the model efficiency by using the Nash-Sutcliffe method (11) to generate coefficients (*E*) for each storm for various contributing areas. This model uses the summations of the absolute squared differences in model predictions and observations to indicate the "closeness" of the model to the system. Values of *E* range from -∞ to1. A value of 1 means that the model is a perfect fit to the observed data, and a value of less than 0 means that the mean of the observed values is more appropriate than model values. The components are: model prediction values (C_{MODEL}); observed values (C_{OBS}); and the mean of the observed values (C_{MEAN}) [*Krause and Boyle*, 2005].

$$E = 1 - \frac{\sum_{i=1}^{n}(C_{MODEL} - C_{OBS})^2}{\sum_{i=1}^{n}(C_{OBS} - C_{MEAN})^2} \quad (11)$$

3.6 - Assumptions

The model makes several assumptions and values taken from literature. First, the mixing model assumes complete mixing in a known volume. Flow paths through the hyporheic zone tend to be laminar as opposed to turbulent, which is what would be required in a well-mixed volume. Next, the contributing areas for both the vertical and horizontal inputs may change with time, and therefore the discharge passing through those areas would change as result in addition to changes in discharge from changes in storm intensity. Next, the soil sample used for the moisture release curve analysis had to be taken from downstream of the study site, and due to the highly heterogenous nature of the riparian soils in WS1, the soil characteristics of the sample may not be accurately representative of the study column soil characteristics. Therefore, the coefficients derived from the soil moisture release curve analysis may be non-representative for the study column. Next, the K_{sat}, value used in the model calculations was a value provided from lab analysis and may not be representative of the shallow soil in the study column. Additionally,

we used the coefficients provided by the lab moisture release curve analysis which were determined from the same soil sample as the K_{sat} value. The lab K_{sat} = 1.85 x 10^{-5} (cm/s) is an order of magnitude smaller than K_{sat} values associated with loam soils where K_{sat} = 6.95 x 10^{-4} (cm/s), according to *Dingman* [2008]. Lastly, the fitting coefficient was fixed for all storms which assumes a fixed hyporheic zone volume. Additionally, we feel that the analyses and model are limited because we did not include the following: pH which has an impact on water chemistry; residence time of the soil water; and mixing volume within the hyporheic zone.

4. Results:

4.1 - Data Observations

To get a general picture of any trends or patterns in CO_2 concentrations in the study column I plotted the deep, shallow, well F2, surface and stream CO_2 probes with stream stage height versus time [Figure 17]. There are some fluctuations in CO_2 concentrations that appear to have some relationship with stream stage height. The stage height changes during storms and seasonality. The maximum and minimum CO_2 concentration values of all probes change as the season progresses. At the beginning of the study period the maximum and minimum CO_2 concentration values are farther apart than at the end of the time of study. For example, the shallow CO_2 minimum is ~4,000 ppm in late November and rises above 10, 000 ppm a few days later in December. Later in mid-March the shallow CO_2 is ~7600 and rises to ~8300 after a few days. The vadose zone CO_2 concentrations decrease for a period of time and then rise again, and the hyporheic CO_2 begins at concentrations much lower than the vadose zone CO_2 concentrations and rise towards the vadose zone concentrations over the course of the study period. The hyporheic CO_2 concentration trends I observed differ from the trends observed in similar studies [*Dosch*, 2014]. The hyporheic CO_2 concentrations begin the wet season at an

average concentration of ~3000 ppm and rise to ~6000 ppm during storms early in the wet season.

Soil CO_2 concentrations were higher at the onset of the wet season and decreased as the season progressed because some of the deciduous trees lose their leaves reducing photosynthetic root respiration, air and stream temperatures decrease, and respiration decreases. The CO_2 concentrations in the vadose zone and the hyporheic zone respond similarly to storm events but from different starting point concentrations [Figure 17]. The magnitudes of the hyporheic CO_2 concentration storm responses appear to be slightly greater than the vadose CO_2 concentration storm responses early in the wet season. As previously stated, the SH CO_2 and D CO_2 concentrations stay relatively close together, but the F2 CO_2 concentration starts off much lower and rises as the season progresses. While located in saturated soil that may be at the base of the capillary fringe rising above the hyporheic zone, the D CO_2 concentrations are not identical to the hyporheic zone CO_2 concentrations. This may indicate a lack of mixing between the vadose zone and the hyporheic zone before the onset of the wet season.

The SH CO_2 and D CO_2 concentrations were similar during the transitional period as well, but the F2 CO_2 concentration was at a low point during Storm 4 after receiving higher concentrations [Figure 17]. The relatively short decreasing trend may have been from groundwater with a lower dissolved CO_2 concentration entering the hyporheic zone resulting in dilution. After this low point, F2 CO_2 concentrations rose again towards the SH CO_2 and D CO_2 concentrations as the season progressed. The wet period is characterized by all CO_2 probes responding to storm events in relative unison and lower stream pCO_2 concentrations [Figure 17].

I decided to model the soil column by focusing on six storms (indicated by red boxes labeled 1-6) that occurred during the wet season. The time periods for the storms were chosen

based on storm events or data availability for analysis and do not cover the same amount of time. The data is presented here as individual dots, but is described in the following text as a “line”.

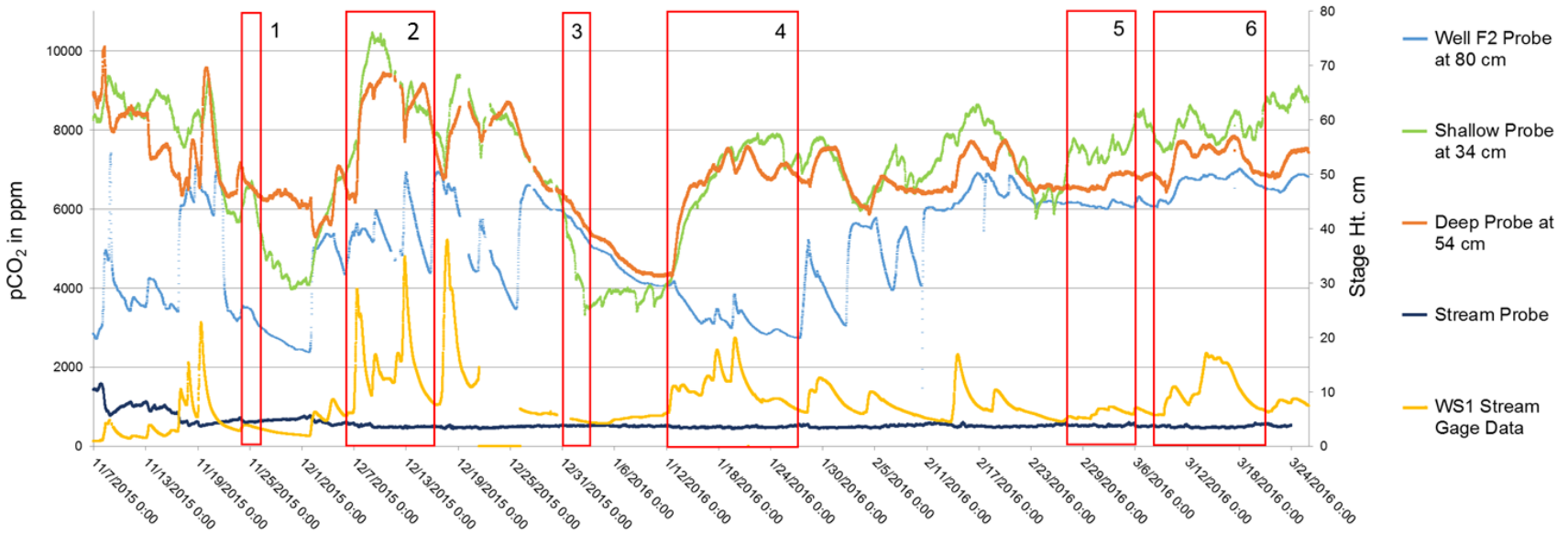

Figure 17: Storms of interest during wet season. The CO_2 concentrations observed at three depths are indicated by different colored markers: “well F2” probe is blue; “deep probe” is orange; “shallow probe” is green; and the “stream probe” is dark blue. The storm intensity is indicated by the stage height data represented by the yellow markers.

4.1.1 - Well F2 CO_2 Concentration:

Well F2 CO_2 concentrations have a general pattern earlier in the wet season that changes as the season progresses. The well F2 concentration (F2 CO_2) starts off much lower than the deep (D CO_2) and shallow (SH CO_2) vadose zone concentrations early in the season on November 7th. The F2 CO_2 looks similar to the stage until mid-February where it begins to resemble with the SH CO_2 and D CO_2 concentrations. Additionally, F2 CO_2 is generally lower than SH CO_2 and D CO_2 until mid-February where it rises to concentrations slightly lower than SH CO_2 and D CO_2. Generally, the F2 CO_2 appears to be influenced by the hyporheic flow for the early part of the wet season, and then influenced by the vadose zone for the latter part of the season. Additionally, the F2 CO_2 concentration begins the wet season at lower values and rise as the season progresses. Hyporheic influence on well F2 CO_2 concentrations can be tested but is beyond the scope of this study, but vadose influence on well F2 CO_2 concentrations is within the scope of this study and will be investigated.

4.1.2 - Shallow and Deep CO_2 Concentration:

The SH CO_2 and D CO_2 concentrations track with each other for the entire wet season with some variance in the relationship. While the concentrations track similarly with each other, the timing and shape of the peaks and troughs do not match exactly. The D CO_2 concentration begins the wet season at values often higher than SH CO_2 concentrations but then falls below SH CO_2 concentrations late in the wet season. Overall, the SH CO_2 and D CO_2 values drop significantly during the middle of the wet season in January, and following this dip they rise again with the D CO_2 values remaining lower than the SH CO_2.

4.2 - van Genuchten K(Θ) and Soil Hydrology:

Results from the Bouwer Rice slug test and lab soil sample analysis suggest that the soil column is comprised of two distinct soil layers with different K_{sat} values. The hyporheic zone has a K_{sat} value two orders of magnitude greater than the vadose zone i.e. horizontal K_{sat} hyporheic zone = 5.7 x 10^{-3} cm s^{-1} and vertical K_{sat} vadose zone = 1.9 x 10^{-5} cm s^{-1}. Additionally, the vadose zone *K* value changes with soil moisture following the van Genuchten model. The changing soil moisture also affects when there is percolation from the vadose zone into the hyporheic zone. I found that the soil column had to be completely saturated down to the deep soil moisture probe for percolation to occur following Bernoulli's equation (12) where elevation head becomes the driving force once pressure head reaches zero. Once there was infiltration, the mixing model was activated using the flux from the vadose zone and the flux from the hyporheic zone. Storms 2, 4, and 6 achieved complete percolation of water from the vadose zone into the hyporheic zone.

4.3 - Changes in Pressure Head and Vadose Zone Model Activation:

Complete percolation depends on vadose zone pressure head values which are dependent on soil moisture, and changes in stream stage height indicate storm events. In my simulation, pressure head (*P*) rises steeply towards zero at the onset of the storm, plateau and then fall again, or experience intermittent troughs in the plateau [Figure 18, A-C]. The starting points of *P* for each storm indicate soil moisture accumulation. As the wet season progresses the soil moisture at the beginning of each storm increases and *P* decreases: Storm 2 initial *P* = -9000 cm; Storm 4 initial *P* = -7800 cm; and Storm 6 initial *P* = -3000 cm. Conversely, the stage height maximums for each of these storms decreased as the season progressed with Storm 2 stage height max = 30

cm and 35 cm; Storm 4 stage height max = 18 cm and 20 cm; and Storm 6 stage height max = 17 cm.

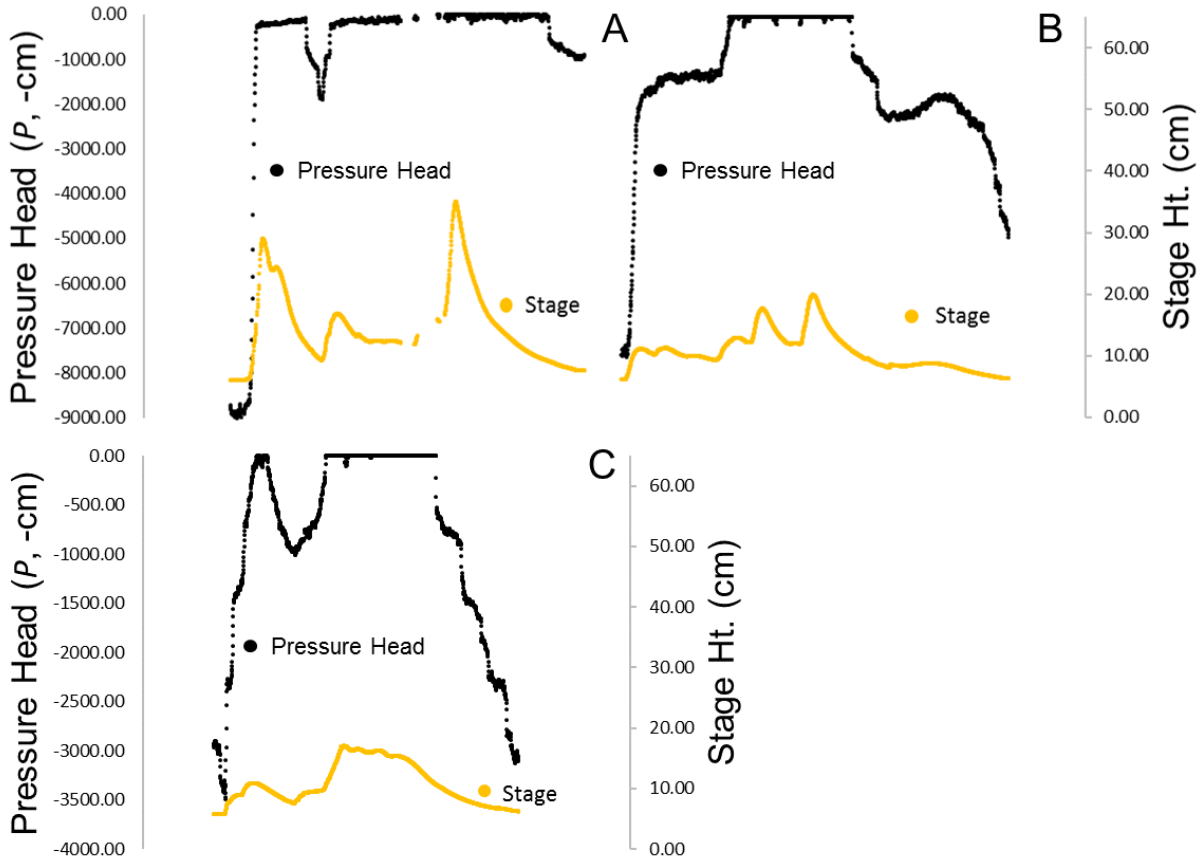

Figure 18. Storms 2 (A), 4 (B), 6 (C) change in pressure head with stage height. Pressure head (P, -cm) is represented by the black data points, and stage height (cm) is represented by the yellow lines.

Figure 19 shows the stage dependent hyporheic zone discharge and the vadose zone hydrological model activating and de-activating during storm events 2, 4, and 6. The maximum discharge occurs during vadose zone saturation resulting in a value of 9.26 x 10^{-6} m^3/s. Storm 2 vadose zone model discharge data points below the maximum discharge value are numerous and varied throughout the course of the storm. Storm 4 vadose zone model discharge data points

below maximum discharge are varied as well, but are fewer in number than Storm 2 sub-maximum discharge value points. Storm 6 vadose zone model discharge data points are mostly at the maximum discharge value with some points falling below. Overall, Figure 19 shows the frequencies of sub-maximum and maximum discharges in the vadose zone during the wet season.

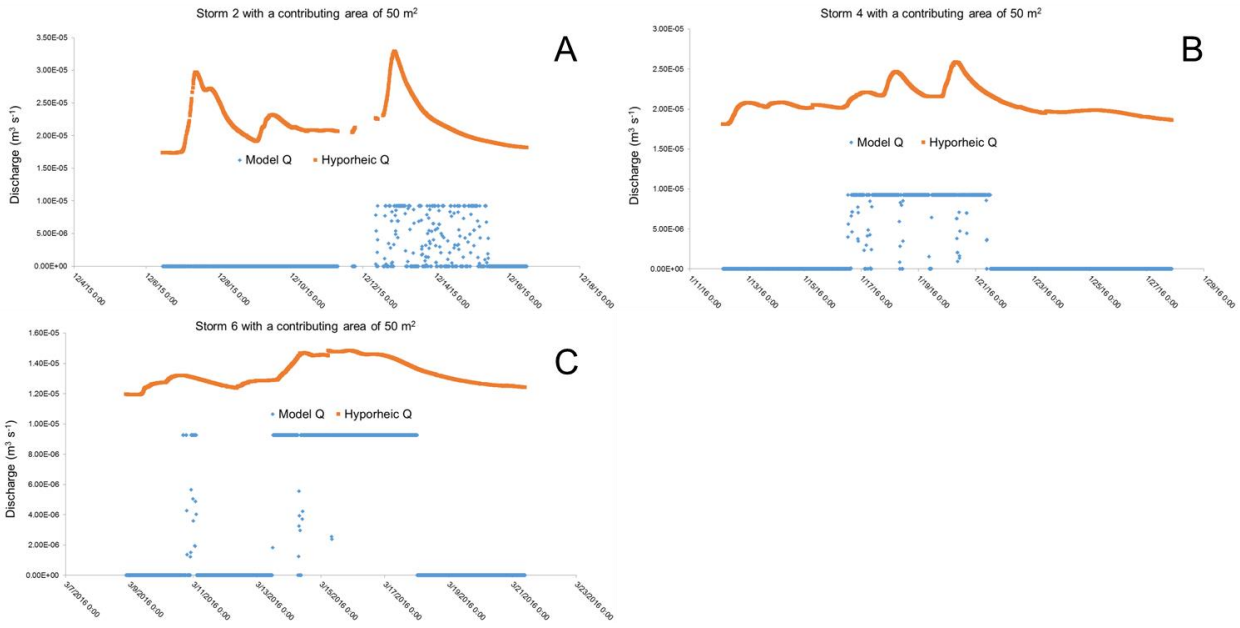

Figure 19. Vadose zone hydrological model activation for storms 2, 4 and 6 (A-C respectively). All storms use a contributing area of 50 m^2. Each simulation uses the same contributing area of 50 m^2 and K_{sat} = 1.85 x 10^{-5} cm s^{-1} for each storm. Each storm activates during the storm event and de-activates as the storm intensity decreases.

4.4 - Storm 2:

Figure 20 shows a plot of model results for Storm 2 with a contributing area of 1 m^2 using the input values listed in Table 1. The input hyporheic CO_2 concentration is fixed at 4.58 mg/L. The simulated dissolved CO_2 concentration in well F2 was fairly constant at ~4.58 mg/L and did

not correctly predict temporal dynamics. The model initiates before the highest peak in stage around midday on 12/12/15, and stops in the afternoon of 12/15/15 on the falling limb of the storm hydrograph. The stage height maximum during model activation was ~35 cm. Storm 2 has the greatest *E* value at a contributing area of 1 m^2, but decrease non-linearly with increasing contributing area [Figure 21] [Table 2]. The largest contributing area values used in Figure 21 are not realistic but were included to advance the model output values towards D CO_2 limit [Figures 32-36, Appendix C].

Storm 2

Parameter	Hyporheic K_{sat} (cm s^{-1})	Vadose K_{sat} (cm s^{-1})	Inverse Air Entry Pressure α (cm^{-1})	m (n=1.4)	Fitting Coefficient, C_f
Value	$5.67*10^{-3}$	$1.85*10^{-5}$	0.00085	0.285714	1.89
Parameter	Q_1 (M^3 s^{-1})	C_1 (mg L^{-1})	Q_2 (M^3 s^{-1})	C_2 (mg L^{-1})	Contributing Area (m^2)
Value	changes with stage ht.	4.58	changes with Θ	observed	1.0

Table 1. Model input values.

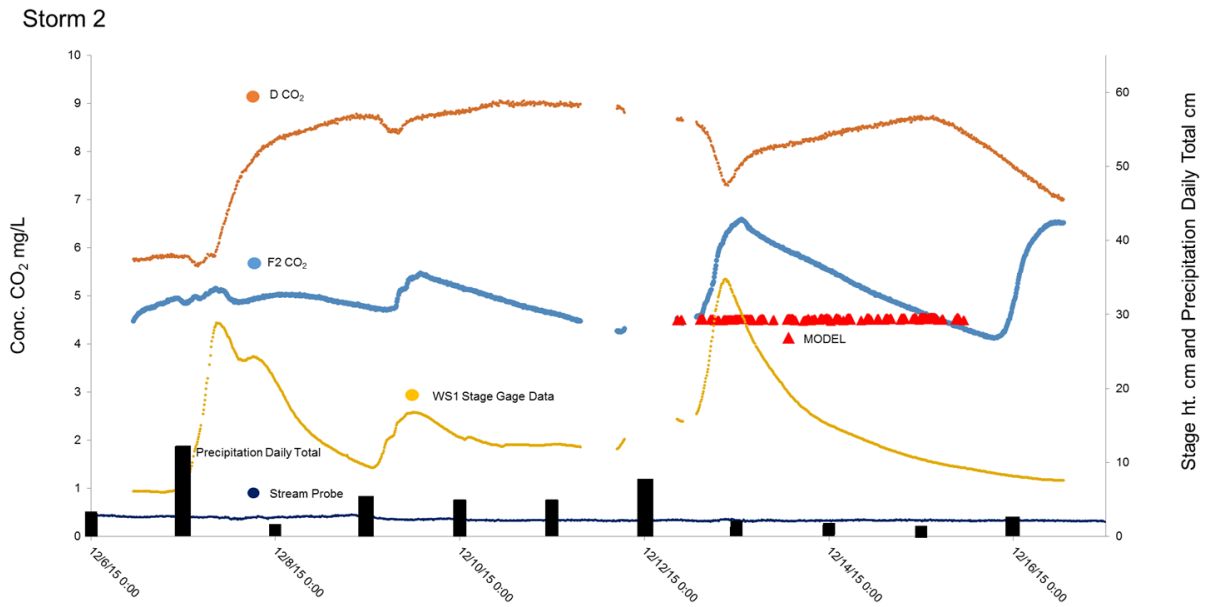

Figure 20. Storm 2 with a contributing area of 1 m^2. The yellow line is the stage height (cm), the black columns are daily precipitation totals (cm), the orange line is the D CO_2 concentration (mg/L), the blue line is the well F2 CO_2 concentration (mg/L), the dark blue line is the stream CO_2 concentration (mg/L), and the model (mg/L) is depicted as red triangles. The well F2 CO_2 concentration line is the target line that the model should match. The SH CO_2 data has been omitted from the following plots because they were not used in any model calculations. The stream CO_2 data has been included as a visual comparison for the well F2 CO_2 concentrations. Precipitation data from Mack Creek rain gauge PPTGSM02 downloaded from H.J. Andrews website. All following model plots [Figures 22 and 24] have the same configurations as Figure 20. Tables 1, 3, and 5 list the model input values for storms 2, 4, and 6. Tables 2, 4, and 6 list the *E* coefficients and contributing areas for storms 2, 4, and 6.

Johnson, S.; Rothacher, J. 2016. Stream discharge in gaged watersheds at the Andrews Experimental Forest, 1949 to present. Long-Term Ecological Research. Forest Science Data Bank, Corvallis, OR. [Database]. Available: http://andlter.forestry.oregonstate.edu/data/abstract.aspx?dbcode=HF004 (15 June 2017)

Daly, C.; Rothacher, J. 2017. Precipitation measurements from historic and current standard, storage and recording rain gauges at the Andrews Experimental Forest, 1951 to present. H. J. Andrews Experimental Forest. Forest Science Data Bank, Corvallis, OR. [Database]. Available: http://andlter.forestry.oregonstate.edu/data/abstract.aspx?dbcode=MS004 (15 June 2017)

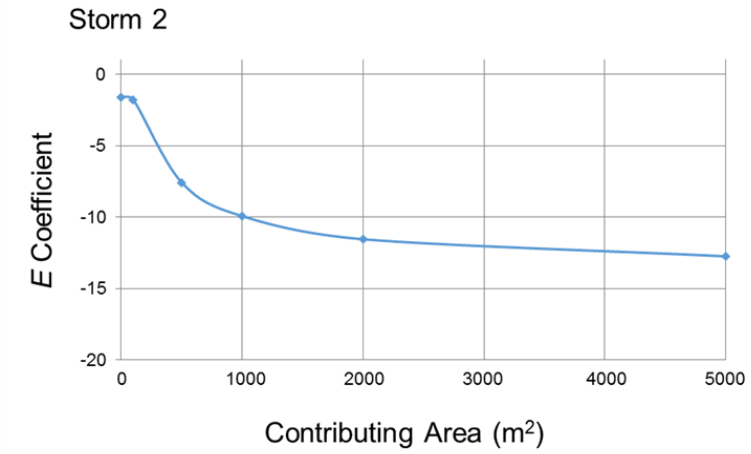

Figure 21. *E* coefficients vs contributing areas (m^2) from the values in Table 2. Contributing areas are increased to such large areas to demonstrate model functionality i.e. the predictions rise towards the D CO_2 line with increasing area. This remains true for all storm simulations.

Storm 2

Contributing Area (m^2)	1	100	500	1000	2000	5000
E Coefficent	-1.616	-1.78	-7.574	-9.928	-11.55	-12.75

Table 2. Storm 2 *E* coefficients with increasing contributing areas.

4.5 - Storm 4:

The Storm 4 change in contributing area analysis was problematic because well F2 CO_2 concentration decreased during the storm [Figure 22]. We decided to use a concentration of 3.0 mg/L as the C_1 input to run the model closer to the observed concentrations as opposed to running the model based on pre-storm concentrations [Table 3]. When changes in area were made, the model either approached the D CO_2 concentration line with increasing area or became smoother with decreasing area [Figures 37-40, Appendix C]. The following are results using a contributing area of 5 m^2 and the fixed hyporheic concentration of 3.0 mg/L. Again, the simulated CO_2 concentration in well F2 was constant over the storm, this time at ~3.5 mg/L. The model pattern poorly matched the observed data, with timing in peaks of observed CO_2 concentrations not matching the simulated "spikes." The model activates during the afternoon of 1/16/16 and stop in the afternoon of 1/21/16 during the falling limb of the stage height line. The stage height maximum during model activation was ~18 cm. The Storm 4 *E* coefficients decrease initially, and then increase with increasing contributing area [Figure 23] [Table 4].

Storm 4

Parameter	Hyporheic K_{sat} (cm s^{-1})	Vadose K_{sat} (cm s^{-1})	Inverse Air Entry Pressure α (cm^{-1})	m (n=1.4)	Fitting Coefficient, C_f
Value	$5.67*10^{-3}$	$1.85*10^{-5}$	0.00085	0.285714	1.89
Parameter	Q_1 ($M^3 S^{-1}$)	C_1 ($mg L^{-1}$)	Q_2 ($M^3 S^{-1}$)	C_2 ($mg L^{-1}$)	Contributing Area (m^2)
Value	changes with stage ht.	3.0	changes with Θ	observed	5.0

Table 3. Model input values.

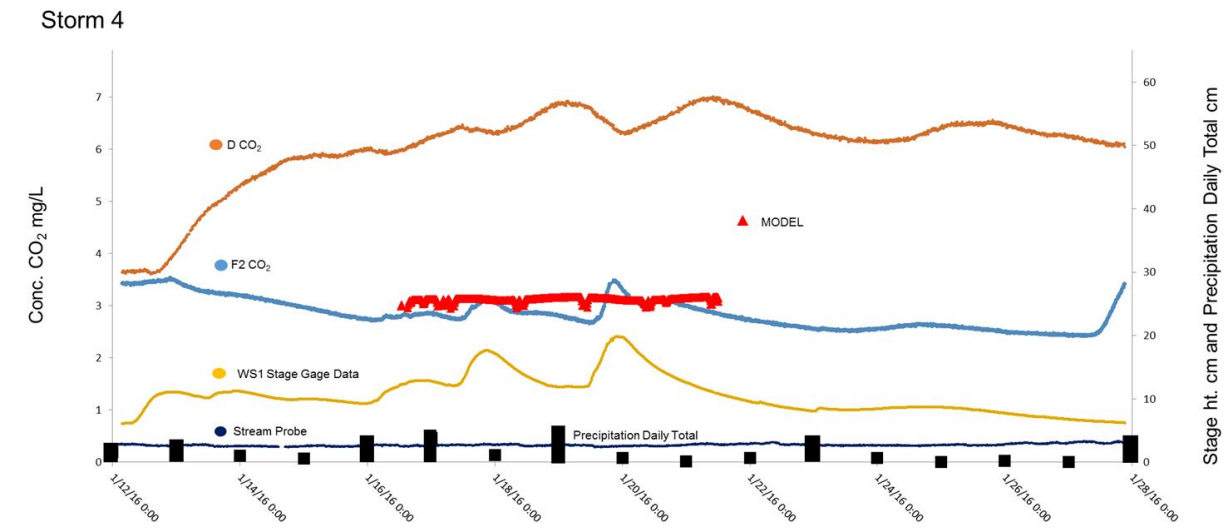

Figure 22. Storm 4 with a contributing area of 5 m^2.

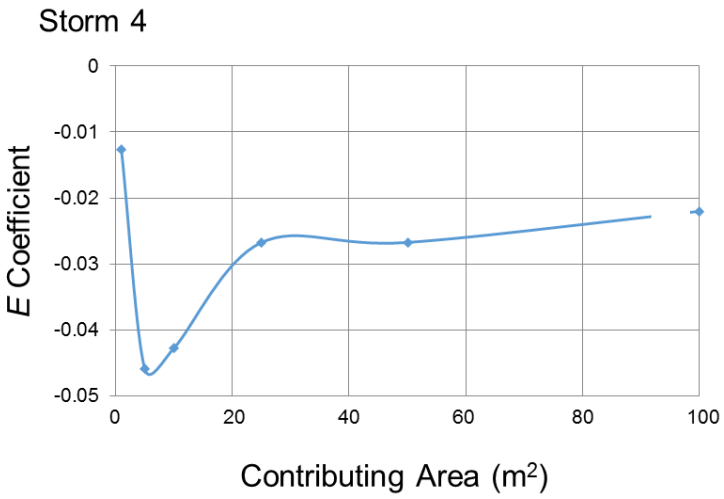

Figure 23. *E* coefficients vs contributing area.

Storm 4

Contributing Area (m^2)	1	5	10	25	50
E Coefficent	-0.013	-0.046	-0.043	-0.027	-0.022

Table 4. Storm 4 *E* coefficients with increasing contributing areas.

4.6 - Storm 6:

The model activates briefly on 3/10/16 and for a longer duration starting around midday on 3/13/16 and stopping around midnight on 3/17/16. The stage height maximums during the first and second events are ~11 cm and ~17 cm respectively [Figure 24]. The model uses the fixed hyporheic CO_2 concentration of 5.74 mg/L, and the contributing area was changed to 25 m^2, 50 m^2, 85 m^2, 95 m^2, 150 m^2, and 500 m^2 which resulted in an upwards shift in model data points towards the D CO_2 concentration line [Figures 39-45, Appendix C]. The model has the best fit with the target line when the contributing area is ~65 m^2 with an *E* coefficient value of 0.21 [Figure 25]. When the contributing area is increased to 500 m^2, the model lands on the D CO_2 concentration line, and will not cross it as area increases. As before simulated values were relatively constant over time, but this time so were the observed values. Figure 25 values are listed in Table 6.

Storm 6

Parameter	Hyporheic K_{sat} (cm s^{-1})	Vadose K_{sat} (cm s^{-1})	Inverse Air Entry Pressure α (cm^{-1})	m (n=1.4)	Fitting Coefficient, C_f
Value	$5.67*10^{-3}$	$1.85*10^{-5}$	0.00085	0.285714	1.89
Parameter	Q_1 (M^3 s^{-1})	C_1 (mg L^{-1})	Q_2 (M^3 s^{-1})	C_2 (mg L^{-1})	Contributing Area (m^2)
Value	changes with stage ht.	5.74	changes with Θ	observed	65

Table 5. Model input values.

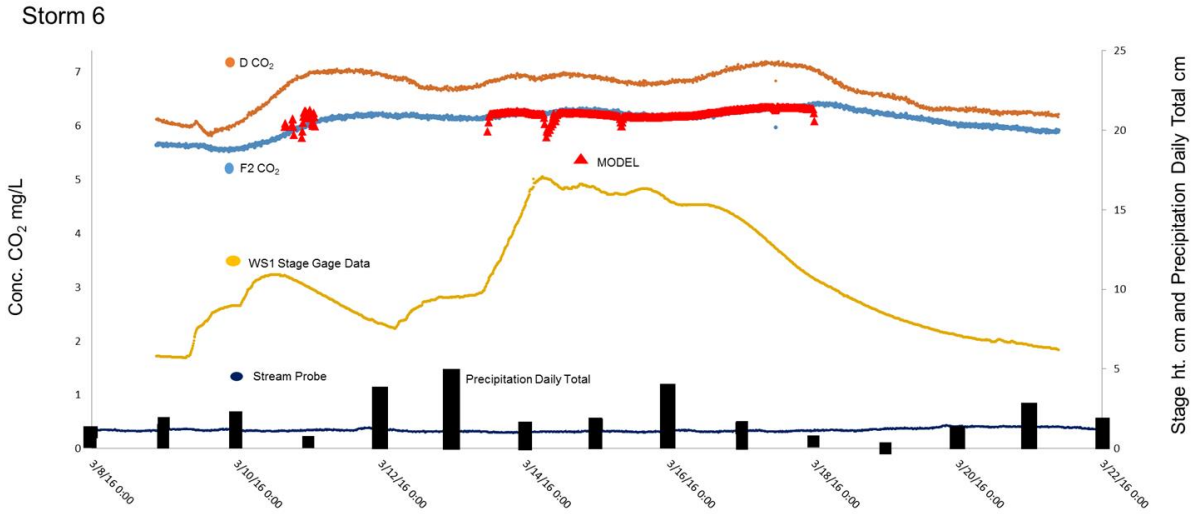

Figure 24. Storm 6 with a contributing area of 65 m^2.

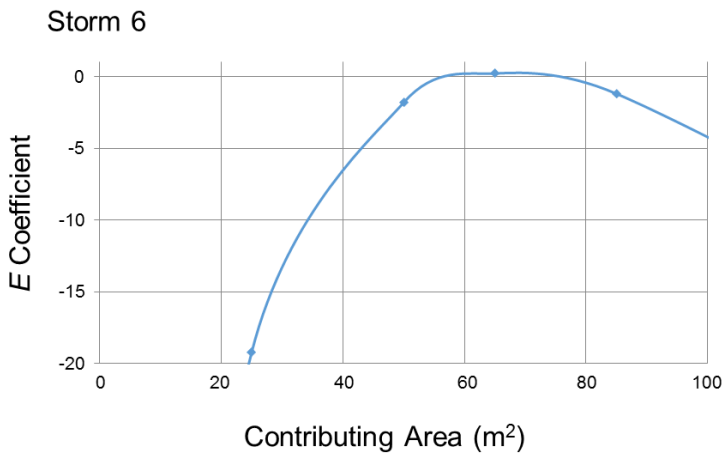

Figure 25. *E* coefficients vs contributing area.

Storm 6

Contributing Area (m^2)	1	25	50	65	85	95	150	250	350
E Coefficent	-83.4	-19.2	-1.81	0.21	-1.2	-2.84	-15.2	-35.89	-50.4

Table 6. Storm 6 *E* coefficients with increasing contributing areas.

4.7 – Model Sensitivity and Verification:

I investigated the sensitivity of the model by adjusting a few model parameters such as: α; m; and K_{sat}. I chose to investigate α and m because we could measure them directly, and were calculated based on the OSUCAL results. I used Storm 6 with a contributing area of 65 m^2 results to compare with changes in α and m. The range of values are in accordance to those presented by *Schaap* [2000] and are located in Tables 7 and 8 in Appendix C. Parameters α and

m had little effect on hyporheic dissolved CO_2 predictions. However; α did affect vadose zone pressure head values resulting in a wider range of data points due to an increase in infiltration time [Figure 46, Appendix C]. The model was sensitive to increases in K_{sat} order of magnitude. When I used the K_{sat} value from *Dingman* [2008] the model results shifted upwards towards the D CO_2 concentration line [Figures 47 and 48, Appendix C], and the model discharge rises above the hyporheic discharge [Figure 49, Appendix C]. I suggest that these results indicate model functionality.

I conducted a sensitivity analysis on the fitting coefficient's role in model calculations by changing the contributing area and K_{sat} values, and then running solver to determine each new fitting coefficient value. Additionally, I used the model results for each contributing area/K_{sat} combination to conduct an *E* coefficient analysis. I found a positive linear relationship between contributing area and the fitting coefficient [Figure 26]. Additionally, I found that increased K_{sat} values result in increased fitting coefficient values. This means that when I increase the vadose zone discharge into the hyporheic zone by increasing the vadose zone K_{sat}, the cross-sectional area component within the fitting coefficient increases causing an increase in hyporheic discharge to maintain the fit between the model output values and the observed values.

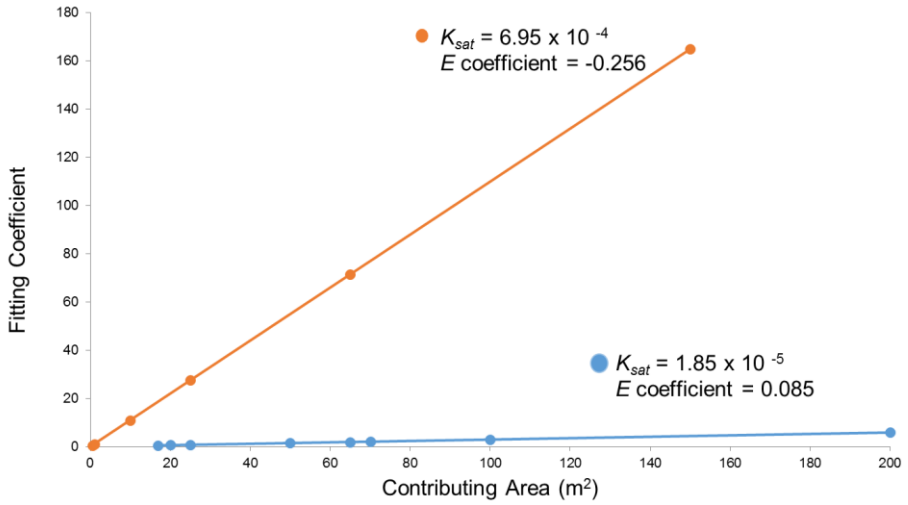

Figure 26. Fitting coefficient sensitivity analysis.

Generally, my fitting coefficient, vadose zone contributing area, and K_{sat} values are all connected and making changes to one means a change in the others. The model uses the same fitting coefficient for all storms in this study which means that I am assuming that the hyporheic zone has the same volume throughout the wet season. I know from literature that this is not the case as described by *Wondzell* [2006]. The model may be more effective if hyporheic zone dimensions are better understood thereby enabling model users to assign an appropriate fitting coefficient. If this was achieved, then modelers could focus on the vadose zone contributing area and subsequent vadose zone dissolved CO^2 contribution to the hyporheic zone.

I verified model calculations by performing a few calculations by hand using values from discrete data points and comparing them to model results with a perfect match. Also, I posit that the contributing area analyses using equation (10) support model performance because of the direct influence that the vadose zone has on equation (11). Additionally, the two contributing sources of dissolved CO_2 to equation (11) represent the two endpoints in the calculations. When I

changed the contributing area the model results landed on or near one of these endpoints. I suggest that the fact that the model is bound by these two endpoints also supports model functionality.

While the model was not useful in making reliable predictions early in the wet season we can still learn from it. The model was designed based on my initial thoughts on what was occurring during rain storms. I initially suspected that dissolved CO_2 was being flushed from the vadose zone into the hyporheic zone in pulses that infiltrate as wetted lenses. The resultant model mixes an infiltration flux and a hyporheic flux producing a final dissolved CO_2 value that I hoped would match observed dissolved CO_2 values. The fact that the model does not produce reliable values early in the wet season tells us that the observed dissolved CO_2 values are not the result of flushing but rather the result of a complicated hyporheic system that is likely quite extensive. Additionally, the model illustrates the complexity of the vadose zone hydrology. A rain event may introduce a significant amount of water to the soil surface but that does not mean that the water will infiltrate to the hyporheic zone. Rather, a series of rain events and accumulated soil moisture can result in complete infiltration. Lastly, the model was fairly simplistic for such a complicated system, but is still useful because it allowed me to gain a better understanding of the primary governing forces occurring in the study column.

5. Discussion:

I expected the model to be able to predict the F2 CO_2 concentration at a given point in time when the vadose zone was sufficiently wet enough to facilitate infiltration of soil water containing dissolved CO_2 into the hyporheic zone. The model resulted in lines that approached the shapes of the observed D CO_2 concentration lines as opposed to the target well F2 CO_2 concentration lines for all storms. I found the study column to be a complex system that cannot

be fully understood using the modeling approach. The findings suggest that the contributing vadose zone volume, which appears to change with time, soil moisture and connectivity, likely has an important role in hyporheic CO_2 concentrations. The following cartoon is a based on the concept in Figure 14, but illustrates a change in time as opposed to a change in moisture [Figure 27].

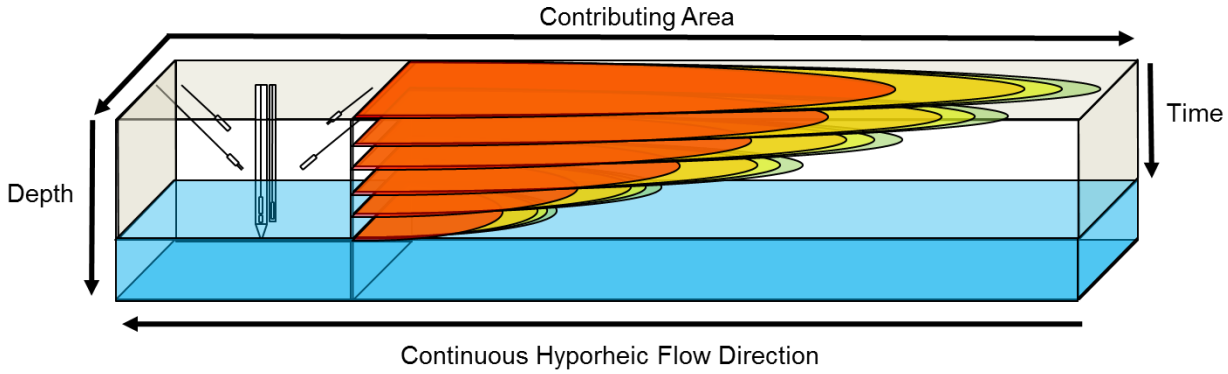

Figure 27. Contributing area change with time. The elongated cubic structure represents the study column and the soil volume upstream of well F2. The blue region in the bottom portion represents the continuous contribution from the hyporheic flow. The contributing area depicted by the colored ellipses change with time and distance from the well F2 instrument cluster shown below on the left. The arrow pointing down indicates a temporal trend in contributing area as the wet season progresses.

5.1 - Dry Period:

I stated previously that the K_{sat} values of the two soil zones that contribute to the model differ by an order of magnitude resulting in a greater contribution of dissolved CO_2 from the hyporheic flow than the vadose zone towards the resultant concentration, C_3. However; the contributing area and *E* coefficient results suggest that the model is not representative of the system early in the wet season, and increasing the contributing area and thus the contribution of

CO_2 from the vadose zone does not improve all model fits. When I increased the contributing area, the *E* coefficients decreased which may support the narrative that the hyporheic zone is isolated from the vadose zone during the dry season. This agrees with a previous study that states that during periods of low flow, the hyporheic zone is sustained by stream water as opposed to contributions from lateral inputs [*Wondzell et al.* 2010]. Furthermore, I found that increasing the contributing area resulted in scattered C_3 values that approached the D CO_2 concentration line.

5.2 - Transitional Period:

As with Storm 2, the model line was not perfectly smooth but rather had a few points that were of higher concentrations, which may indicate a contribution from the vadose zone. However; these points of higher concentration are few enough to question their relevance and therefore contribution from the vadose zone can be considered negligible. The expansion of contributing area increased the C_3 values towards the D CO_2 concentration line but again, this did not improve model fits. In fact, increasing contributing area made the model fits worse.

5.3 - Wet Period:

Increasing the contributing area resulted in model prediction values approaching the D CO_2 observed values. Although most of the *E* coefficient values were negative indicating the utility of using the observed values over the model values, there was a brief period of positive values around a contributing area of 65 m^2 during Storm 6. This indicates that continual increases in contributing area, as in Storm 2, will not yield the best *E* coefficient, but rather there is an ideal contributing area. The positive E coefficient value indicates model effectiveness during the latter part of the wet season as opposed to early in the wet season.

5.4 –Contributing Areas vs E Coefficients, Connectivity, and Mixing:

The contributing areas required to achieve the greatest *E* coefficients may indicate the connectivity of the vadose and hyporheic zones. Figure 19 shows the frequencies of maximum and sub-maximum vadose zone discharges during the wet season. Storm 2 has a higher frequency of sub-maximum vadose zone discharge than Storm 6. I suggest that this indicative of changes in soil connectivity because a higher frequency of maximum discharge is due to soil saturation and water flow from the vadose zone to the hyporheic zone. Furthermore, I suggest that as soil moisture approaches saturation, the dissolved CO_2 contributions observed in well F2 may come from a shorter distance upstream [Figure 25]. I suspect this is because rainwater can infiltrate to the hyporheic zone having passed through the vadose zone while becoming concentrated in dissolved CO_2 at all soil depths. The result is a flow of dissolved CO_2 concentrations from the shallow vadose zone towards the hyporheic zone, and the well F2 observed dissolved CO_2 concentrations are the final product. Furthermore, I suggest that this flow indicates a shallow to deep directionally mixed hyporheic/vadose zone, meaning that it is the vadose zone water percolating down and mixing with the hyporheic zone water and not hyporheic zone water rising and mixing with the shallow portion of the vadose zone.

I also suggest that the opposite may be true. When the soil is less than saturated and connectivity is decreased, dissolved CO_2 observed in the hyporheic zone may be the accumulation of an expansive network of pathways. To be clear, this does not mean that a portion of the dissolved CO_2 observed in the hyporheic zone at times of soil saturation may not also be dissolved CO2 from an expansive contributing area. Generally, I posit that at times of soil saturation, the dissolved CO_2 observed in the hyporheic zone at a given location may be predominantly from the immediate area.

Mixing between the soil layers became an important factor in distributing dissolved CO_2. Infiltration occurring over the course of the wet season resulted in the hyporheic zone displaying the same characteristics as the upper and lower portions of the vadose zone. This mixed relationship appears to begin in mid-February [Figure 17]. Prior to this time, the study column seems to function as two separate systems: the well F2/hyporheic zone; and the deep and shallow soil horizons of the vadose zone. This allows us to picture the hyporheic zone at different times of the year: an expansive network of stream sourced flow paths during the dry season; a changing hyporheic volume during the transitional period; and a connected hyporheic/vadose continuum at times when the vadose zone is saturated.

5.5 - Seasonality, Changes in Pressure Head, and Hysteresis:

The seasonality of the study column during the wet season can be somewhat understood when looking at model results: the hyporheic zone is not connected to the vadose zone during the dry period; the hyporheic zone is transiently connected with the vadose zone during the transitional period; and vadose zone water is at times percolating into the hyporheic zone during the wet period. The decrease in stage height with each successive storm event indicates less precipitation and therefore less rainwater landing on the soil surface. As the wet season progresses the dry soil retains some of the moisture from each storm event until it becomes saturated enough for percolation. The effect of storm intensity on percolation was also observed in a similar study conducted in Watershed 10 in the H.J. Andrews [*van Verseveld et al*., 2008]. Researchers found that flow direction in the unsaturated soil depended on storm intensity, and the heavy storm events resulted in percolation of rainwater through the soil [*van Verseveld et al*., 2008].

Soil water accumulation occurs from forces that promote soil moisture retention [*Selker, J. et al*., 1999]. The rainwater is the "new" water while the soil water is the "old" water. The increasing pressure head, increasing soil moisture, and decreasing storm intensity promote percolation more readily during the latter part of the wet season. The study column may be displaying counter-clockwise hysteresis pattern where the new water volume required for percolation from the vadose zone to the hyporheic zone decreases over the course of the wet season [*Selker et al*., 1999].

5.7 - Further Study:

As previously stated, a complete analysis should include the gas transport out of the system because it could allow researchers to be able to describe the hyporheic/vadose/atmosphere continuum more completely. Soil surface CO_2 evasion is a continuous process and would likely be influenced by storm events during the wet season as soil moisture changes thereby effecting gas movement and respiration. Monitoring soil surface evasion may enable researchers to determine when CO_2 evasion ceases and CO_2 storage begins. Furthermore, increasing soil moisture increases the possibility for a reverse concentration gradient becoming a potential contributive source of CO_2 to the hyporheic zone upon saturation. Additionally, a soil gas study may be able to indicate whether there is a Birch effect at the end of the dry season which may prove useful when analyzing gaseous CO_2 production within the vadose zone. A more complete set of observational data and analysis of these processes could allow researchers to determine the timing, duration and impact of each process.

Soil water DOC/DIC can be investigated through storm sampling thereby enabling researchers to determine respiration and CO2 productivity during periods of increased hyporheic discharge. System wide water contributing sources may be determined using electrical

conductivity probes deployed at various depths and locations upstream of the monitored well. Furthermore, carbon species in soil and hyporheic water can be determined using pH probes deployed at various depths and locations upstream of monitored well.

Monitoring the soil moisture gradient can become more precise with the deployment of additional moisture probes for a more continuous moisture profile. However; installation of a sufficient number of probes may be too destructive to the soil column thereby altering natural structures and creating artificial flow paths. In addition to soil moisture probes, a cluster of continuous measurement soil pressure probes could be useful for cross-checking the calculated pressure values. The study could also be made to include a larger data set from a network of probes and wells. Perhaps the study should still focus on the central well but using the surrounding data points as system boundaries creating dynamic planes of influence.

5.7.1 - End Member Mixing Analysis:

An End Member Mixing Analysis (EMMA) would have been a useful addition to this study. An EMMA could have helped determine the source(s) of water moving through the system and helped us identify old soil water; new rain water; hyporheic water; and ground-water. The utility of knowing the percentages of various packets of water is that it can indicate the connectivity of the system. For instance, during the described dry period I believe the system to be comprised of two layers that rarely interact with each other. The vadose zone is very dry and the CO_2 concentrations are much higher, while the hyporheic zone has CO_2 concentrations that are much lower than the vadose zone. As previously stated, when I increased the contributing area for Storm 2 I believe the increased area to mean increased hyporheic flow paths as opposed to an increase in vadose zone surface area contribution. An EMMA could have allowed me to determine the kind(s) of water was passing through the hyporheic zone during Storm 2 i.e.,

hyporheic water, groundwater, soil water, new water, or most likely a combination. For example, a previous study found that gas evasion was at times interrupted by periods of lateral pCO_2 transport during saturation. An EMMA could have allowed me to determine the source(s) of the water and therefore the processes that contributed to the resultant observed pCO_2 concentration.

However; EMMA analyses require samples taken from the source. The experimental design was based on continuous dissolved CO_2 observations from several depths and to acquire these samples I would have used suction cup lysimeters to extract water samples containing dissolved CO_2. The problem with this technique is that the lysimeters use a vacuum to pull the sample from the soil solution, but this is a problem for the pressure sensitive pCO_2 [*Brezonik and Arnold*, 2012]. During sampling, suction cup lysimeters create preferential flow paths thereby sampling a small area around the porous cone rather than passively sampling the water flowing through the area. Additionally, they have a relatively short time frame (~24 hours) for collection due to head loss in the sampler, and as the data is continuous, the sample would only be a snapshot in time of soil dissolved CO_2 as opposed to an observation point recording the dynamic patterns of dissolved CO_2 with time [*Brandi-Dohrn, F. et a.l*, 1996].

6. Summary:

I hypothesized that storm events promote a "flushing" mechanism of CO_2 stored in the vadose zone into the hyporheic zone. Flushing relies on soil moisture and the connectivity of the soil column during storm events. I modeled the system based on observed dissolved CO_2 concentrations at multiple depths, soil moisture; soil and water temperature at multiple depths; water table height; soil analyses results; and stream stage height. I found that the study column was not a uniform volume of soil but rather a complex system comprised of two layers with different K_{sat}; moisture; dissolved CO_2 concentrations; and connectivity that cannot be

completely described using the model. We suggest that the soil column should be described as a vadose zone overlying a hyporheic zone with seasonally changing connectivity between the two.

I chose to focus my study during the onset of the wet season which enabled me to observe soil characteristics before, during, and after times of saturation. I suggest that the study column can be described as three different periods of time for analysis: dry; transitional; and wet. The inter-connectivity of the study column was seasonal with low connectivity during the dry period and higher connectivity during the wet period. The improving connectivity may be the result of soil water accumulation and counter-clockwise hysteresis. The seasonal trend observations for this study differed than the seasonal trends observed in the study conducted by *Dosch* [2014]. I did not observe the decrease followed by the sudden increase in well F2 CO_2 concentrations at the onset of storms [Figure 1], and the well F2 CO_2 concentration trend was opposite from previous studies conducted in WS1 in that the well F2 CO_2 concentration rose as the wet season progressed as opposed to decreasing [*Dosch*, 2014]. The well of focus in the [*Dosch*, 2014] study was a different well located ~2 meters from my study well F2. Given the heterogeneity of the riparian soil in WS1, it is not very surprising that I did not observe the same storm responses as observed in the [*Dosch*, 2014] study. Additionally, well installation may have been different between the two wells as they were installed at different times resulting in different hydrological storm responses.

The model was useful in determining the timing and of infiltration from the vadose zone into the hyporheic zone, which only occurred during saturation. Another useful contribution of the model was my ability to investigate contributing area changes and the resultant *E* coefficients, which determined model predictions' closeness to the observations. I found that during the dry period the observed data should be considered reliable rather than the model

predictions at all contributing areas. As the wet season progressed and soil moisture increased, I found the required contributing area to be 65 m^2 for an *E* coefficient of ~0.21. I suggest this is because the study column is saturated and new rain water entering through the surface can mobilize dissolved CO_2 and infiltrate through the system more quickly due to increased soil connectivity.

Generally, the model can determine when the soil is sufficiently saturated to allow percolation of water from the surface toward the hyporheic zone based on soil moisture and pressure head, and made reasonable hyporheic dissolved CO_2 predictions in well F2 during Storm 6. Additionally, I suggest that the flow of dissolved CO_2 from the vadose zone into the hyporheic zone may be the result of several of these infiltration events. The findings do not suggest that the vadose zone is a continual source of CO_2 to low order streams, but rather a contributive source over a relatively short time during the wet season.

The results of this study have inspired new questions about vadose/hyporheic exchange. When complete infiltration from the vadose zone into the hyporheic zone occurs, what does this newly saturated column become? A hyporheic zone with water piled on top? A hyporheic zone that extends into what was once the vadose zone? The similar looking well F2 and D CO_2 concentration lines during Storm 6 may indicate that the D CO_2 probe is reading hyporheic zone CO_2 concentrations as opposed to the well F2 CO_2 probe reading deep vadose zone CO_2 concentrations. If this is true then contribution of dissolved CO_2 from the vadose zone to the hyporheic zone may become more convoluted as the definitions of each term need redefining.

7. Conclusions:

Overall, this study illustrates the complexities of a seasonal system, which is additionally confounded by the imperceptible intricacies of contributing factors. My continuous observations were useful but the limited locations of data acquisition, limit the quantitative analysis. I believe that the ability to understand the dynamic nature of the hyporheic zone can aid us when we try to construct a three-dimensional shape that can grow in depth, increase in length, and decrease in width.

- Connectivity from the vadose zone to the hyporheic zone is seasonal.
- The study column can be described as “dry”, “transitional”, and “wet”.
- Dissolved CO_2 contribution from the vadose zone to the hyporheic zone occurs when the soil is sufficiently saturated to enable complete percolation from the vadose zone to the hyporheic zone.
- Prior to complete saturation the system is a complex network with unidentified boundaries

8. Bibliography:

Argerich, A., R. Haggerty, S. L. Johnson, S. M. Wondzell, N. Dosch, H. Corson-Rikert, L. R. Ashkenas, R. Pennington, and C. K. Thomas (2016), Comprehensive multiyear carbon budget of a temperate headwater stream: carbon budget of a headwater stream. *Journal of Geophysical Research: Biogeosciences*, 121(5), 1306–15.

Birch, H.F. (1964), Mineralisation of plant nitrogen following alternate wet and dry conditions. *Plant and Soil*. 1.

Bouwer, H. (1989), The Bouwer and Rice slug test; an update, *Ground Water, 27*(3), 304-309.

Brezonik, P. and W. Arnold (2012), Water chemistry: Fifty years of change and progress, *Environmental Science & Technology*, *46*(11), 5650-7.

Brandi-Dohrn, F., R. P. Dick, M. Hess, and J. S. Selker (1996), Suction Cup Sampler Bias in Leaching Characterization of an Undisturbed Field Soil, *Water Resources Research*, 32(5), 1173–82.

Butman, D., H. F. Wilson, R. T. Barnes, M. A. Xenopoulos, and P. A. Raymond (2014), Increased Mobilization of Aged Carbon to Rivers by Human Disturbance, *Nature Geoscience*, 8(2), 112–16.

Butman, D. and P. Raymond (2011), Significant Efflux of Carbon Dioxide from Streams and Rivers in the United States, *Nature Geoscience*, 4(12), 839–42.

Cole, J., Y. Prairie, T. Caraco, N. McDowell, F. Tranvik, W. Striegl, H. Duarte, L. Kortelainen, R. Downing, G. Middelburg, and C. Melack (2007), Plumbing the Global Carbon Cycle: Integrating Inland Waters into the Terrestrial Carbon Budget, *Ecosystems*, 10(1), 172–85.

Corson-Rikert, H. A. (2014), Carbon Dynamics in the Hyporheic Zone of a Headwater Mountain Stream in the Cascade Mountains, Oregon, Corvallis, Or., Oregon State University.

Dingman, S. (2008), Physical hydrology (2nd ed.), Long Grove, Ill., Waveland Press.

Dosch, N. T. (2014), Spatiotemporal Dynamics and Drivers of Stream pCO_2 in a Headwater Mountain Catchment in the Cascade Mountains, Oregon, Corvallis, Or., Oregon State University.

Downing, J. J., J. Cole, C. M. Duarte, J. M. Middelburg, Y. T. Melack, P. Prairie, R. G. Kortelainen, W. H. Striegl, L. J. Mcdowell, and Ja Tranvik (2012), Global Abundance and Size Distribution of Streams and Rivers, *Inland Waters*, 2(4), 229–36.

Dyrness, C.T. (1977), Hydrologic Properties of Soils on Three Small Watersheds in the Western Cascades of Oregon, USDA Forest Service Research PNW - 111. Portland, Or., Pacific Northwest Forest and Range Experiment Station, U.S. Forest Service.

Harr, R. D. (1977), Water Flux in Soil and Subsoil on a Steep Forested Slope, *ResearchGate*, 33(1–2), 37–58.

Harr, R. D. (1976), Hydrology of Small Forest Streams in Western Oregon, USDA Forest Service General Technical Report PNW; 55. Portland, Or., Pacific Northwest Forest and Range Experiment Station, U.S. Dept. of Agriculture, Forest Service, 1976. http://www.treesearch.fs.fed.us/pubs/22617.

Hope, D., S. M. Palmer, M. F. Billett, and J. C. Dawson (2001), Carbon Dioxide and Methane Evasion from a Temperate Peatland Stream, *Limnology and Oceanography*, 46(4), 847–857.

Jarvis, P., A. Rey, C. Petsikos, L. Wingate, M. Rayment, J. Pereira, J. J. Banza (2007), Drying and Wetting of Mediterranean Soils Stimulates Decomposition and Carbon Dioxide Emission: The 'Birch Effect', *Tree Physiology*, 27(7), 929–940.

Johnson, D., D. Geisinger, R. Walker, J. Newman, J. Vose, K. Elliot, and T. Ball (1994), Soil PCO 2 , Soil Respiration, and Root Activity in CO 2 -fumigated and Nitrogen-fertilized Ponderosa Pine, *Plant and Soil*, 165(1), 129-38.

Johnson, M. S., M. F. Billett, K. J. Dinsmore, M. Wallin, K. E. Dyson, and R. S. Jassal (2009), Direct and Continuous Measurement of Dissolved Carbon Dioxide in Freshwater Aquatic Systems-Method and Applications, *Ecohydrology*. *Ecohydrology*, 3(1), 68-78.

Kasahara, T., and S. M. Wondzell (2003), Geomorphic Controls on Hyporheic Exchange Flow in Mountain Streams. *Water Resources Research*, 39(1), 3-14.

Krause, P., and D. P. Boyle, and F. Bäse (2005), Comparison of Different Efficiency Criteria for Hydrological Model Assessment, *Advances in Geosciences*, 5, 89-97.

Mualem, Y. (1976), A new model for predicting the hydraulic conductivity of unsaturated porous media, *Water Resources Research, 12*(3), 513-522.

Raymond, P. A., J. Hartmann, R. Lauerwald, S. Sobek, C. Mcdonald, M. Hoover, D. Butman, R. Striegl, E. Mayorga, C. Humborg, P. Kortelainen, H. Dürr, M. Meybeck, P. Ciais, and P. Guth (2013), Global Carbon Dioxide Emissions from Inland Waters, *Nature*, 503(7476), 355–59.

Richey, J. E., J. M. Melack, A. K. Aufdenkampe, V. M. Ballester, and L. L. Hess (2002), Outgassing from Amazonian Rivers and Wetlands as a Large Tropical Source of Atmospheric CO2, *Nature*, 416(6881), 617–620.

Rinehart, A., J. B. Jones Jr, and T. K. Harms (2015), Hydrologic and Biogeochemical Influences on Carbon Processing in the Riparian Zone of a Subarctic Stream, *Freshwater Scienc*, 34(1), 222–32.

Schaap, M., and F. Leij (2000), Improved prediction of unsaturated hydraulic conductivity with the Mualem-van Genuchten model, *Soil Science Society of America Journal, 64*(3), 843-851.

Schnoor, J. (1996), Environmental modeling: Fate and transport of pollutants in water, air, and soil, *Environmental science and technology*, New York: Wiley.

Schwartz, F., and H. Zhang, (2003), Fundamentals of ground water. New York: Wiley.

Selker, J., C. K. Keller, and J. T. McCord (1999). Vadose zone processes. Baca Raton, FL: Lewis.

Swanson, F., and M. James (1975), Geology and Geomorphology of the H.J. Andrews, *USDA Forest Service Research PNW - 188*.

Tang, J., L. Misson, A. Gershenson, W. Cheng, and A. H. Goldstein (2005), Continuous Measurements of Soil Respiration with and without Roots in a Ponderosa Pine Plantation in the Sierra Nevada Mountains, *Agricultural and Forest Meteorology*, 132(3–4), 12–27.

van Genuchten, M. (1980), A Closed-Form Equation for Predicting the Hydraulic Conductivity of Unsaturated Soils, *Soil Science Society of America Journal*, 44(5), 892-898.

van Verseveld W. J, J. J. Mcdonnell, and K. Lajtha (2008), A Mechanistic Assessment of Nutrient Flushing at the Catchment Scale, *Journal of Hydrology*, 358(3), 268-87.

Wondzell, S. (2006), Effect of Morphology and Discharge on Hyporheic Exchange Flows in Two Small Streams in the Cascade Mountains of Oregon, USA, *Hydrological Processes*, 20(2), 267–87.

Wondzell, S.M., M. N. Gooseff, and B. L. McGlynn (2010), An Analysis of Alternative Conceptual Models Relating Hyporheic Exchange Flow to Diel Fluctuations in Discharge during Baseflow Recession, *Hydrological Processes*, 24(6), 686–94.

Appendix A: Nomenclature

α Inverse air entry pressure ($0.0001 < \alpha < 1.000$) [Schaap, 2000]

m Function of pore size distribution n ($1.0001 < n < 10$) ($9.99 \times 10^{-5} < m < 0.9$) [Schaap, 2000]

h Total head in cm

z Elevation head in cm

θ_S Saturated soil moisture ($60.0\ \phi < \theta_S < \phi$ $m^3\ m^{-3}$), where ϕ = total porosity [Schaap, 2000]

θ_r Residual soil moisture ($0.0 < \theta_r < 30.0$ $m^3\ m^{-3}$) [Schaap, 2000]

θ_{Obs} Observed soil moisture in $m^3\ m^{-3}$

K_{Sat} Saturated hydraulic conductivity in cm s^{-1}

Q Discharge in $m^3\ s^{-1}$

C Dissolved CO_2 concentration in mg L^{-1}

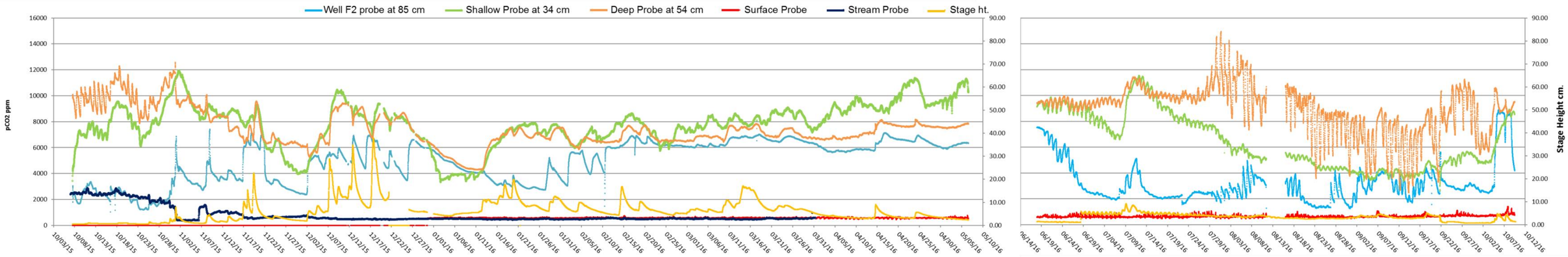

Figure 28. Full year plot 10/2015 - 10/2016. The CO_2 concentrations observed at three depths are indicated by different colored markers: “well F2” probe is blue; “D CO_2 probe” is orange; “SH CO_2 probe” is green; the “stream probe” is dark blue, and the surface CO2 probe is the red line. The stage height is the yellow line. The CO2 concentrations are in ppm and the stage height is in centimeters. There is missing data from 05/10/2016 – 06/14/2016.

Appendix B: Methods additional materials

Survey Data Plot

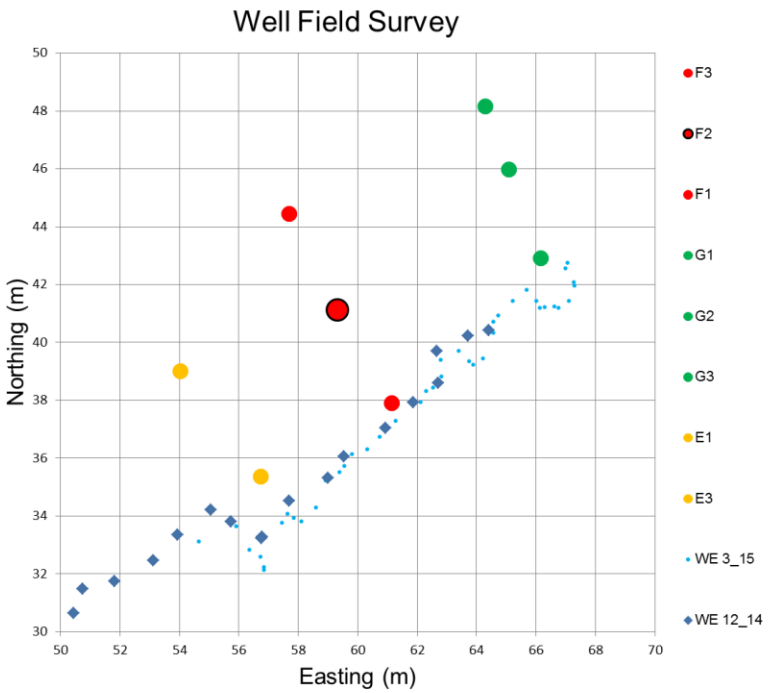

Figure 29: Survey data used to determine $\frac{\partial h}{\partial z}$ for hyporheic K_{Sat}. The red circle with the black outline is well F2 and the other colored dots are other wells in the well field. The blue diamonds and blue dots are survey points for Northing, Easting and elevational data taken at different times. The grid is made up of 4 m^2 boxes.

Pressure Transducer Model for Missing Data

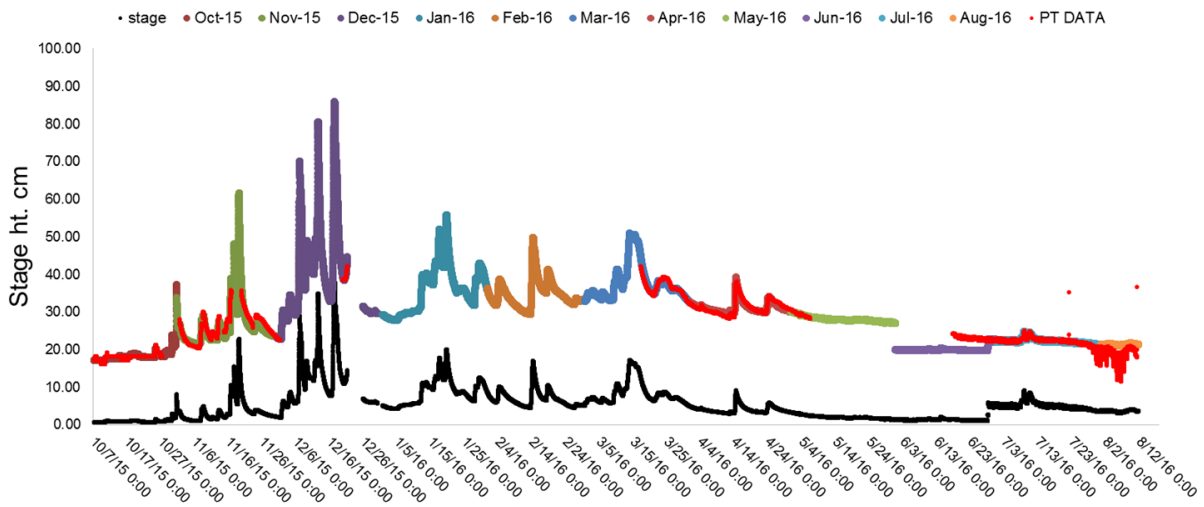

Figure 30. Pressure transducer model with observed data. The stage height data is the black line, the pressure transducer data is represented by the red lines, and the missing portions of pressure transducer data is represented by colored lines. There is missing pressure transducer data so a simple model based on stage height was used to fill in the gaps.

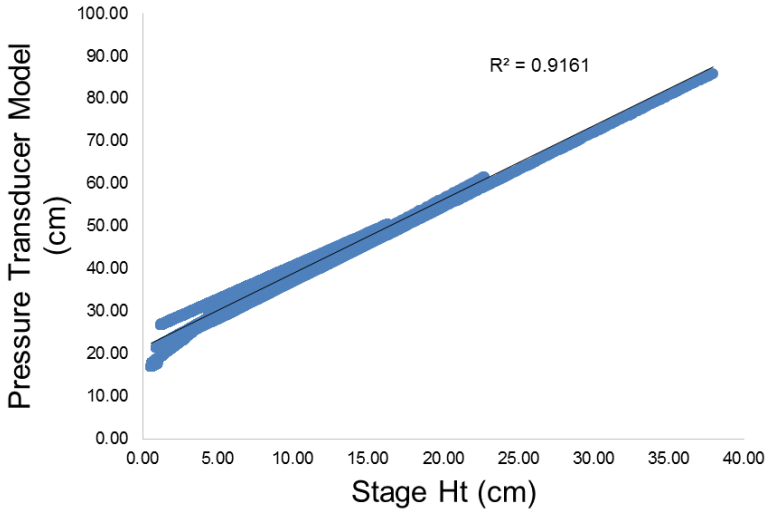

Figure 31. Pressure transducer model vs stage height plot. The pressure transducer missing data vs pressure transducer observed data yielded an $R^2 = 0.916$.

Total Head and Discharge Calculations

The change in total head (∂h) was calculated using equation (12) using: pressure head in -cm (P); and elevation head in cm (Z) [*Schwartz and Zhang*, 2003].

$$h = P_1 + Z_1 = P_2 + Z_2 \tag{12}$$

I calculated the flow in (m^3/s) through each zone of our soil column using Darcy's equation (13) using: hydraulic conductivity in cm/s (K); area of flow in m^2 (A), the change in total head between locations in centimeters (cm) (∂h); and the change in elevation or distance in meters (∂Z) [*Schwartz and Zhang*, 2003]. Following typical convention, negative values indicate downward flow and positive values indicate upward flow.

$$Q = -KA\frac{\partial h}{\partial Z} \tag{13}$$

Slug Tests

I used the Bower and Rice method for a slug test conducted at well F2 following the procedure described by *Bouwer* [1969]. The components for the Bouwer Rice method (14) and (15) are: hydraulic conductivity (K); length of screened portion of well (L_e); length of well below water table (L_w); radial distance to undisturbed soil (r_w); radial distance effected by inside of well water levels and outside of well water levels (R_e); depth of water from datum (H); time (t); water level at time zero (Y_o); inside radius of well (r_c); and water level at time (Y_t) [*Bouwer*, 1969].

$$\ln\left(\frac{R_e}{r_w}\right) = \left[\frac{1.1}{\ln\left(\frac{L_w}{r_w}\right)} + \frac{A+B\ln\left(\frac{(H-L_w)}{r_w}\right)}{\frac{L_e}{r_w}}\right]^{-1} \tag{14}$$

$$K = \left(\frac{{r_c}^2 \ln\left(\frac{R_e}{r_w}\right)}{2L_e}\right)\frac{1}{t}\ln\left(\frac{Y_0}{Y_t}\right) \tag{15}$$

Model Chemistry

I used Henry's equation to convert the partial pressure of CO_2 (pCO_2) in µatm to the dissolved concentration in mg/L (16). The components are: aqueous concentration in mg/L (C_{aq}); gas concentration in atmospheres (C_{gas}); and the Henry's coefficient in L*atm*mol^{-1} (Kh_T).

$$C_{aq} = \frac{C_{gas}(\text{atm})}{K_{h_T}\left(\frac{\text{L atm}}{\text{mol}}\right)} = \text{mol/L} \tag{16}$$

The Henry's coefficient is temperature dependent and needs to be corrected [*Brezonik and Arnold*, 2012]. I used the van't Hoff (17) for Henry's coefficient temperature correction where $K_h^0 = 29.41\ at\ 20\ C$; the coefficient C is defined by (16); and the temperature (T) is in Kelvin as well as the initial temperature (T^o) [*Brezonik and Arnold*, 2012].

$$K_h(T) = K_h^0 \exp^{\left(C\left(\frac{1}{T}-\frac{1}{T^O}\right)\right)} \tag{17}$$

I used (18) to determine the value for the change in enthalpy to use in (19) in accordance with (Reaction 1) to determine the enthalpy of formation products and reactants following methods used in [*Brezonik and Arnold*, 2012].

$$\Delta H^O = \sum H_f^O, products - \sum H_f^O, reactants \tag{18}$$

$$H_2O + CO_2 \longleftrightarrow H_2CO_3$$

Reaction 1.

I made the following calculation for the change in enthalpy based on (Reaction 1):

$$\Delta H^O = H_f^O(H_2CO_3) - \left(H_f^O(H_2O) + H_f^O(CO_2)\right)$$

$$\Delta H^{O} = -20.37\left(\frac{\text{kJ}}{\text{mol}}\right) = -699.7\left(\frac{\text{kJ}}{\text{mol}}\right) + 285.83\left(\frac{\text{kJ}}{\text{mol}}\right) + 393.5\left(\frac{\text{kJ}}{\text{mol}}\right)$$

I calculated coefficient C to be used in (16) using (19) where R is the ideal gas constant in (J mol^{-1} K^{-1}) [*Brezonik and Arnold*, 2012]:

$$C = \frac{\Delta H^{O}}{R}(K) \tag{19}$$

$$\frac{\Delta H^{O}}{R}(K) = -20.37\left(\frac{\text{kJ}}{\text{mol}}\right)\left(\frac{1000\text{J}}{\text{kJ}}\right)\left(\frac{\text{mol K}}{8.314\text{ J}}\right) \approx 2400\ K$$

I calculated the temperature correction from 20 ºC to 9.65 ºC for the Henry's coefficient using the following methods:

$$K_h(\text{T}) = K_h(9.65 + 273) = 29.41\left(\frac{\text{L atm}}{\text{mol}}\right)\exp\left(2400\text{ K}\left(\frac{1}{282.65\text{K}} - \frac{1}{298\text{K}}\right)\right) = 45.55\left(\frac{\text{L atm}}{\text{mol}}\right)$$

Appendix C: Results additional materials

Contributing Area

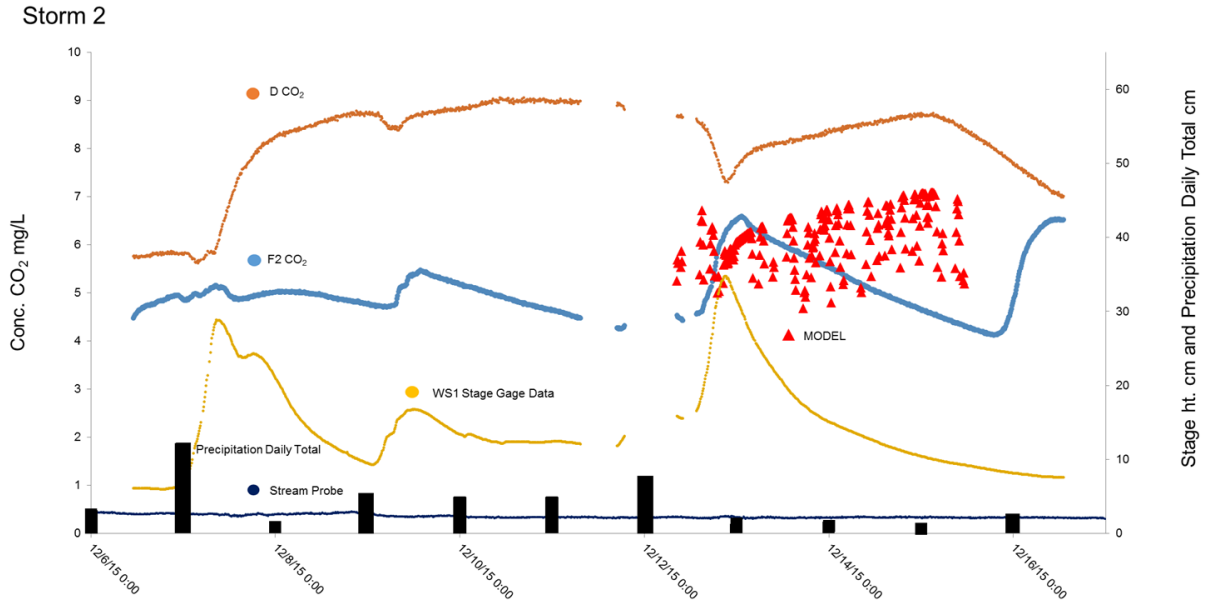

Figure 32: Storm 2 with a contributing area of 100 m^2.

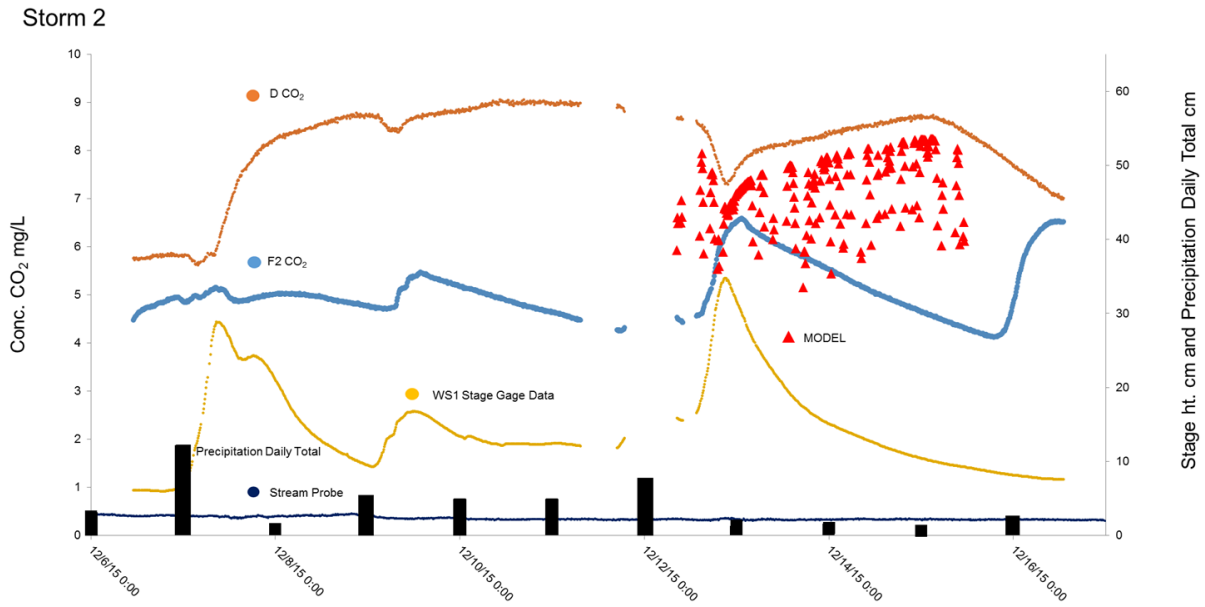

Figure 33: Storm 2 with a contributing area of 500 m^2.

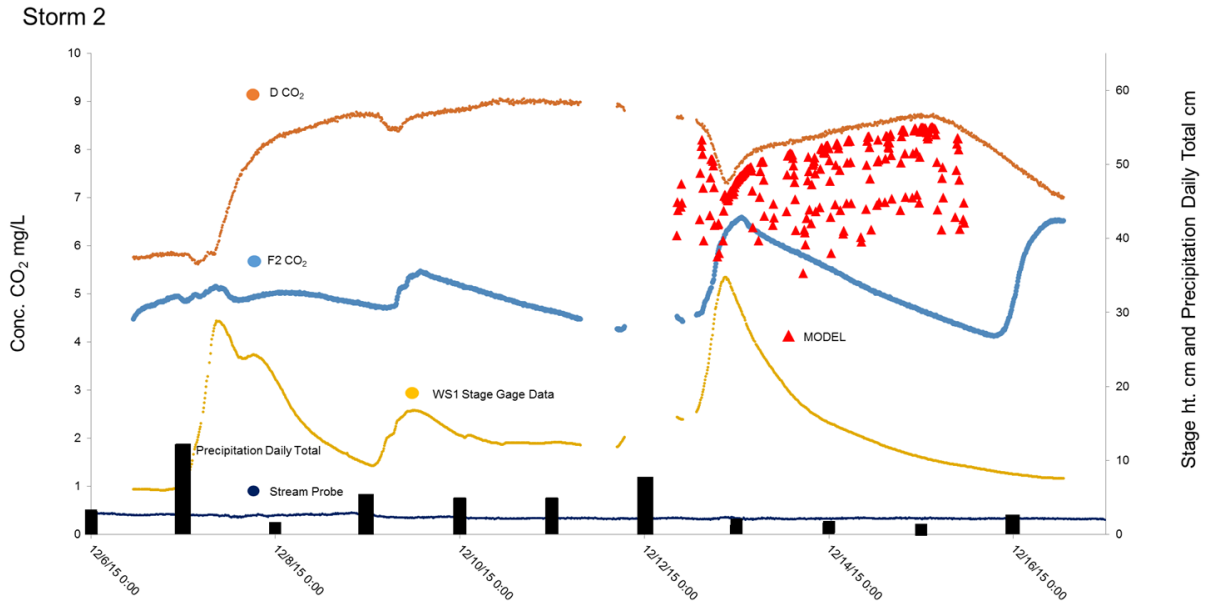

Figure 34: Storm 2 with a contributing area of 1000 m^2.

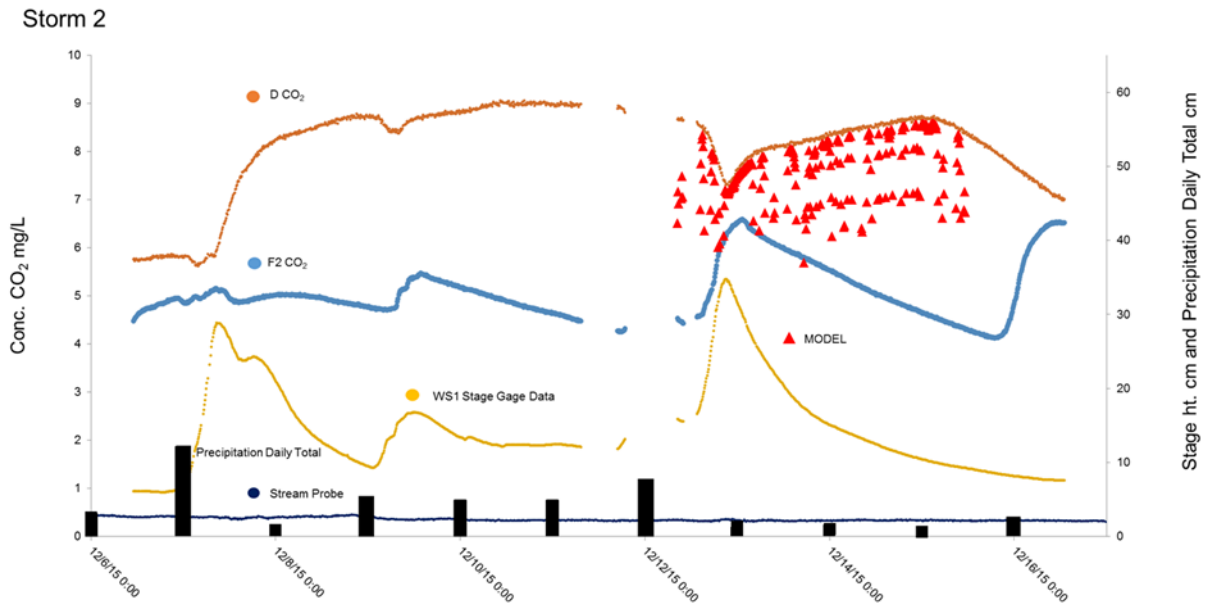

Figure 35: Storm 2 with a contributing area of 2000 m^2.

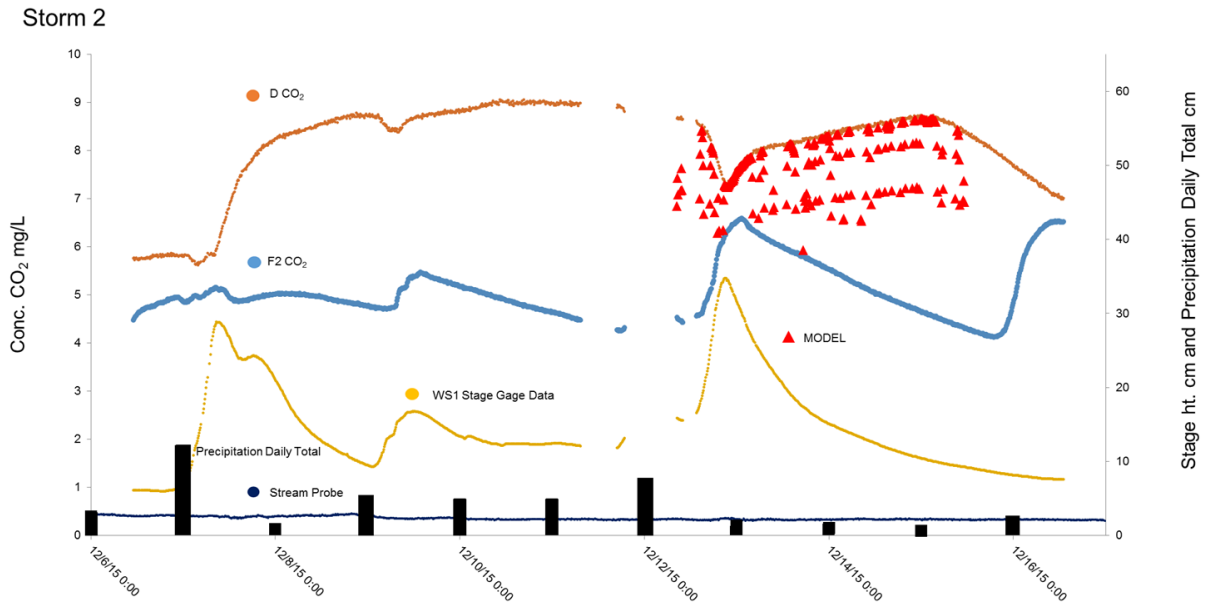

Figure 36: Storm 2 with a contributing area of 5000 m^2.

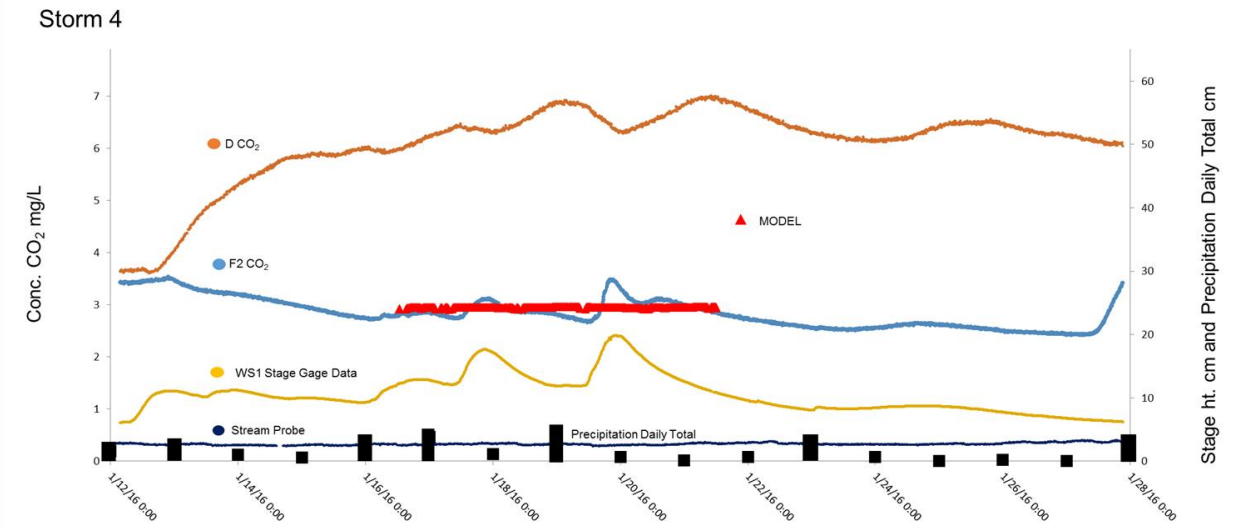

Figure 37: Storm 4 with a contributing area of 1 m^2.

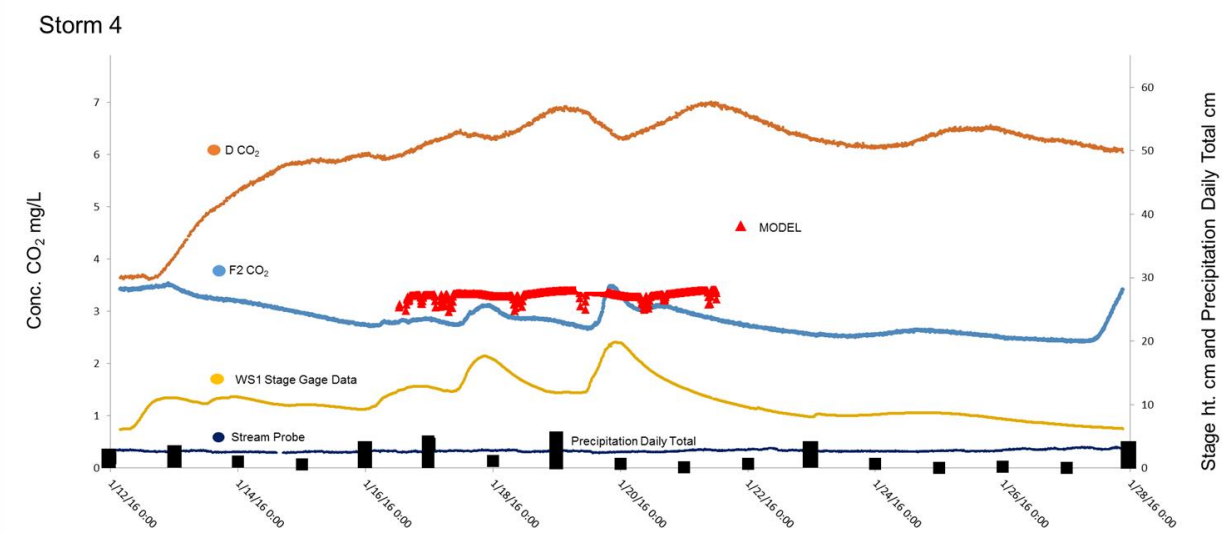

Figure 38: Storm 4 with a contributing area of 10 m^2.

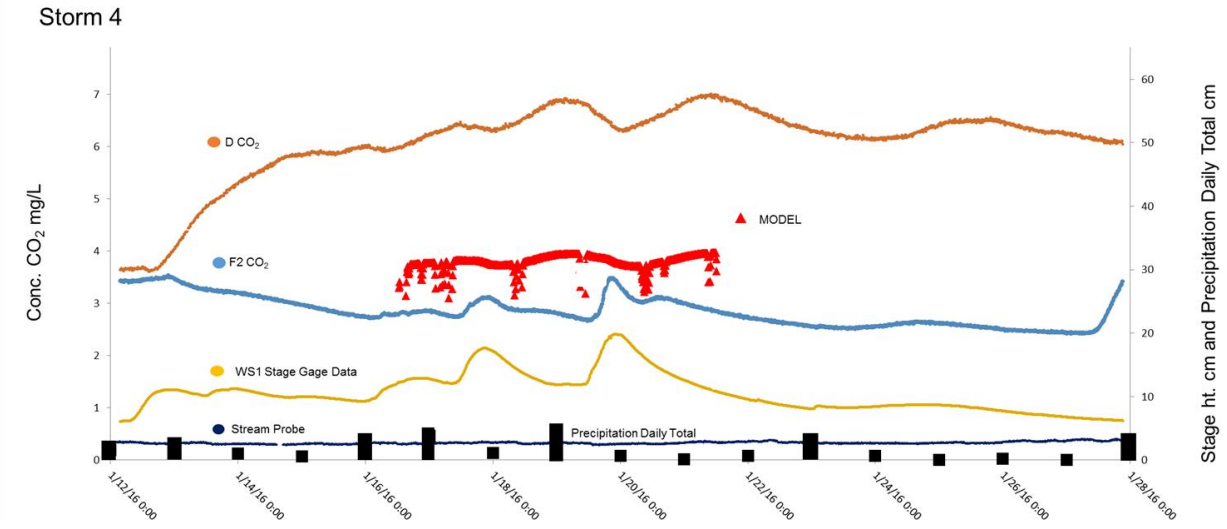

Figure 39: Storm 4 with a contributing area of 25 m^2.

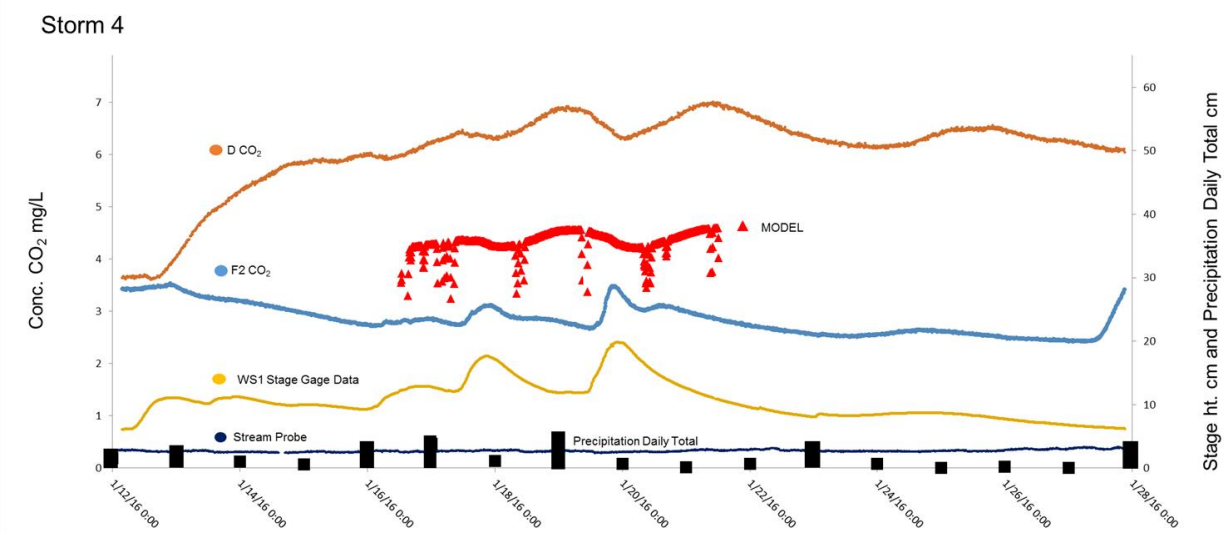

Figure 40: Storm 4 with a contributing area of 50 m^2.

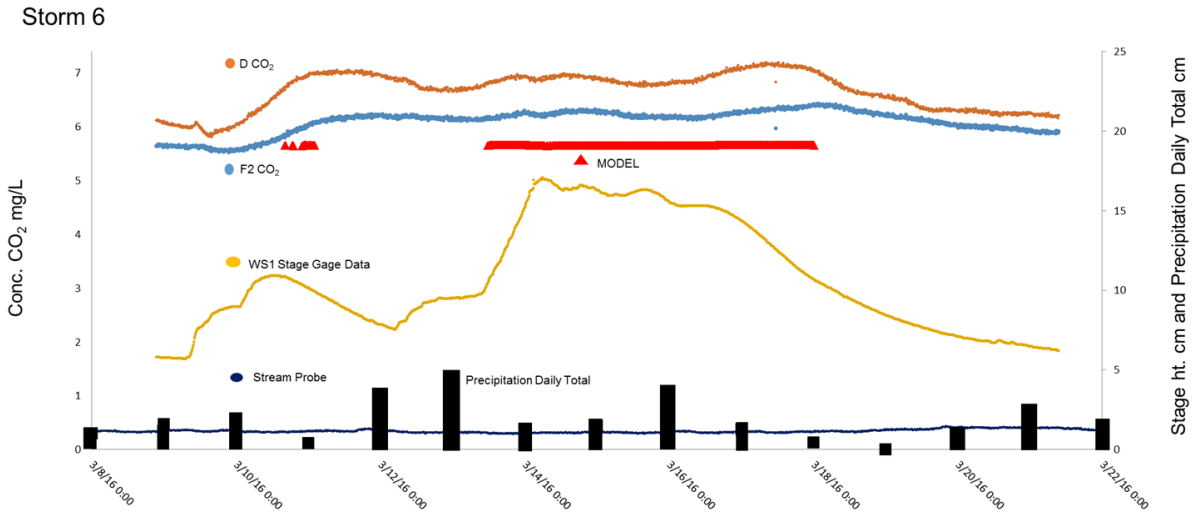

Figure 41: Storm 6 with a contributing area of 1 m^2.

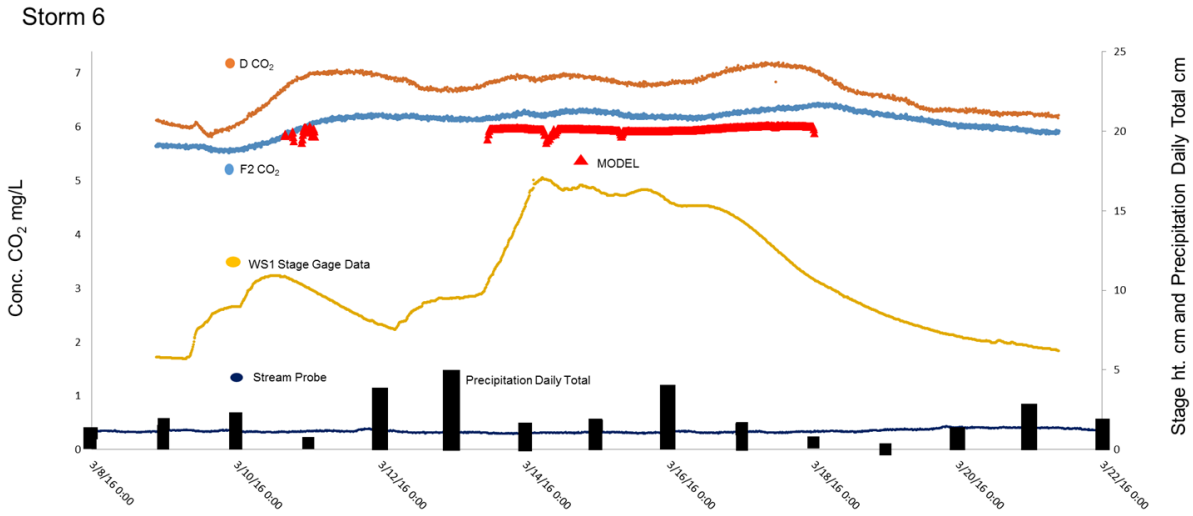

Figure 42: Storm 6 with a contributing area of 25 m^2.

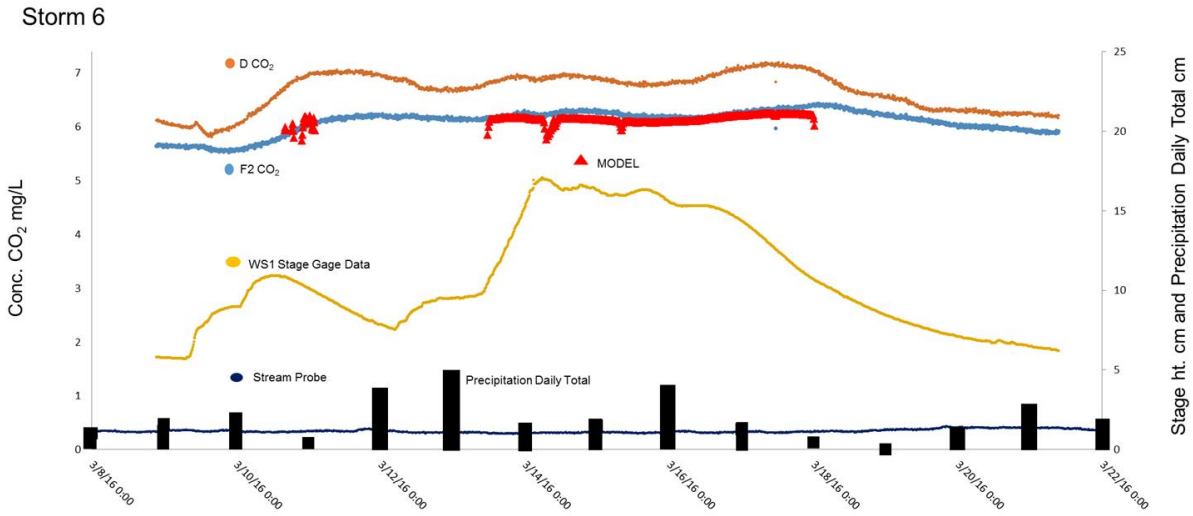

Figure 43: Storm 6 with a contributing area of 50 m^2.

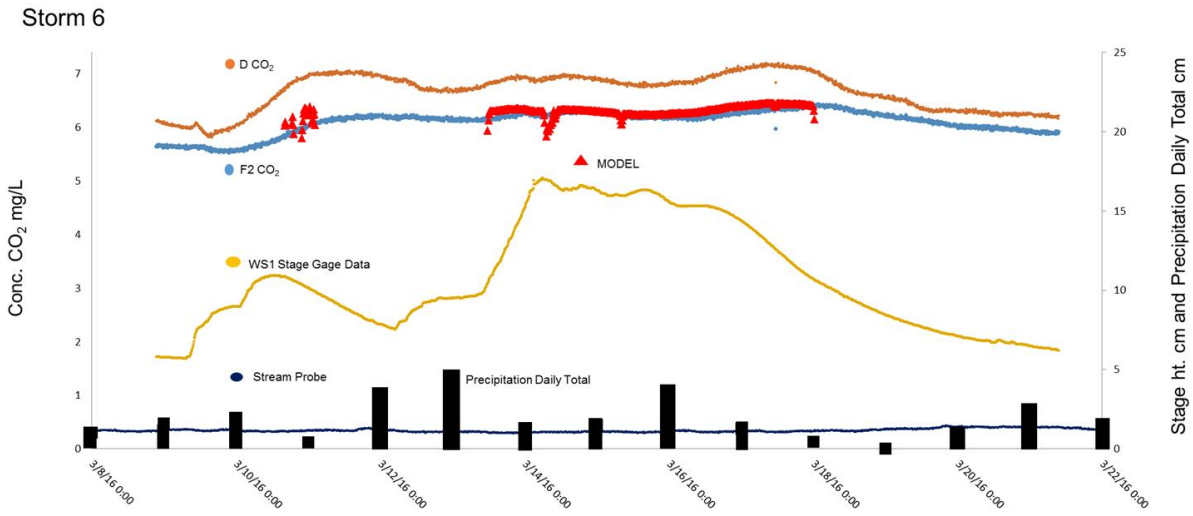

Figure 44: Storm 6 with a contributing area of 85 m^2.

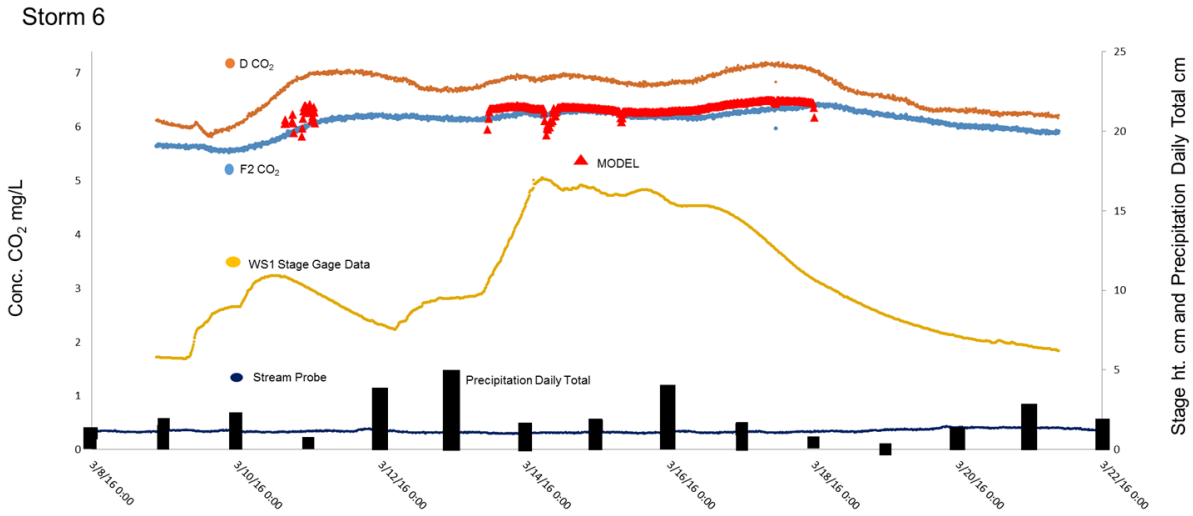

Figure 45: Storm 6 with a contributing area of 95 m^2.

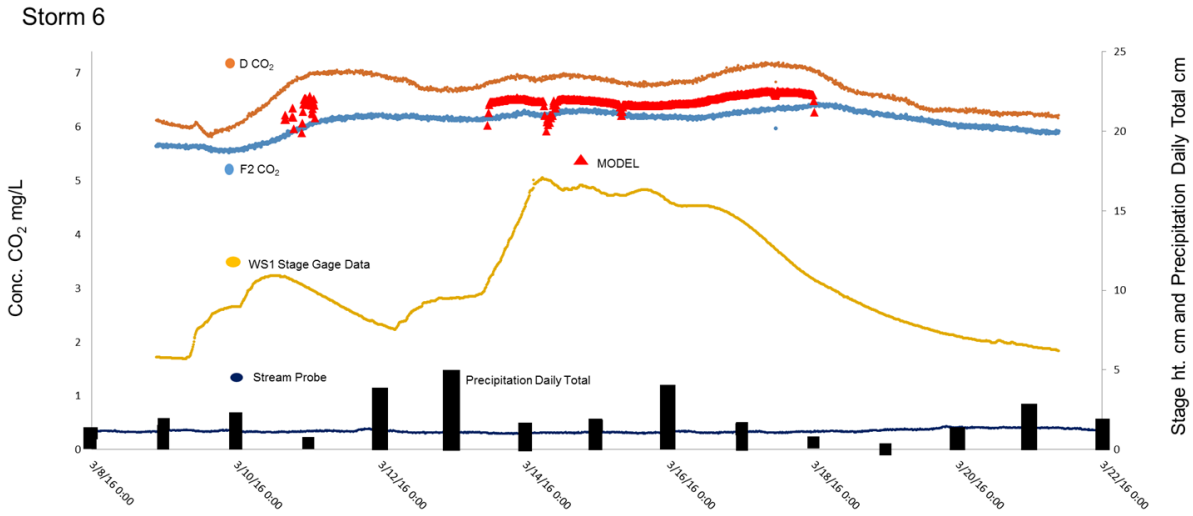

Figure 46: Storm 6 with a contributing area of 150 m^2.

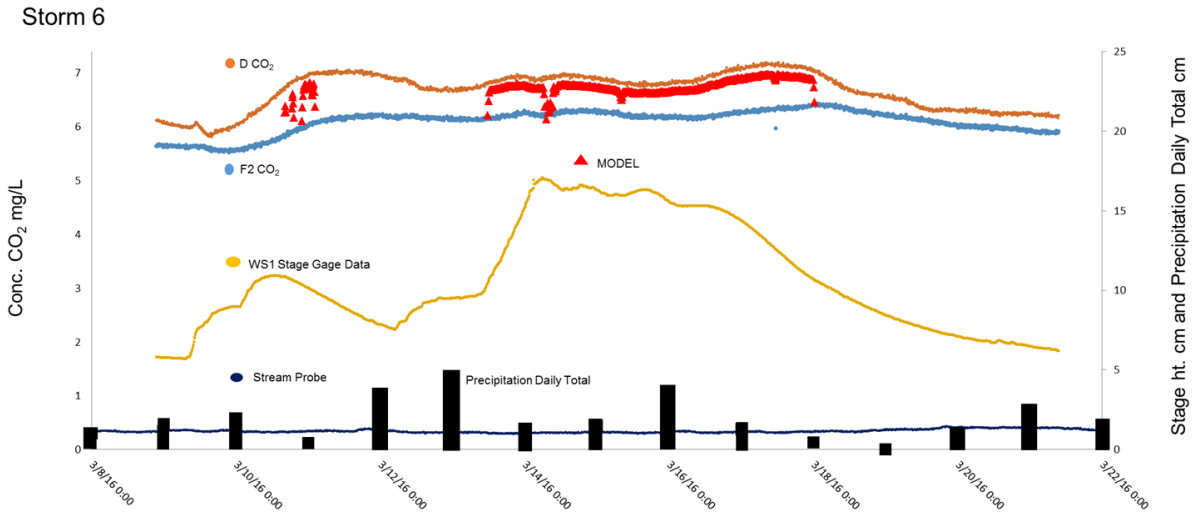

Figure 47: Storm 6 with a contributing area of 500 m^2.

Model Sensitivity

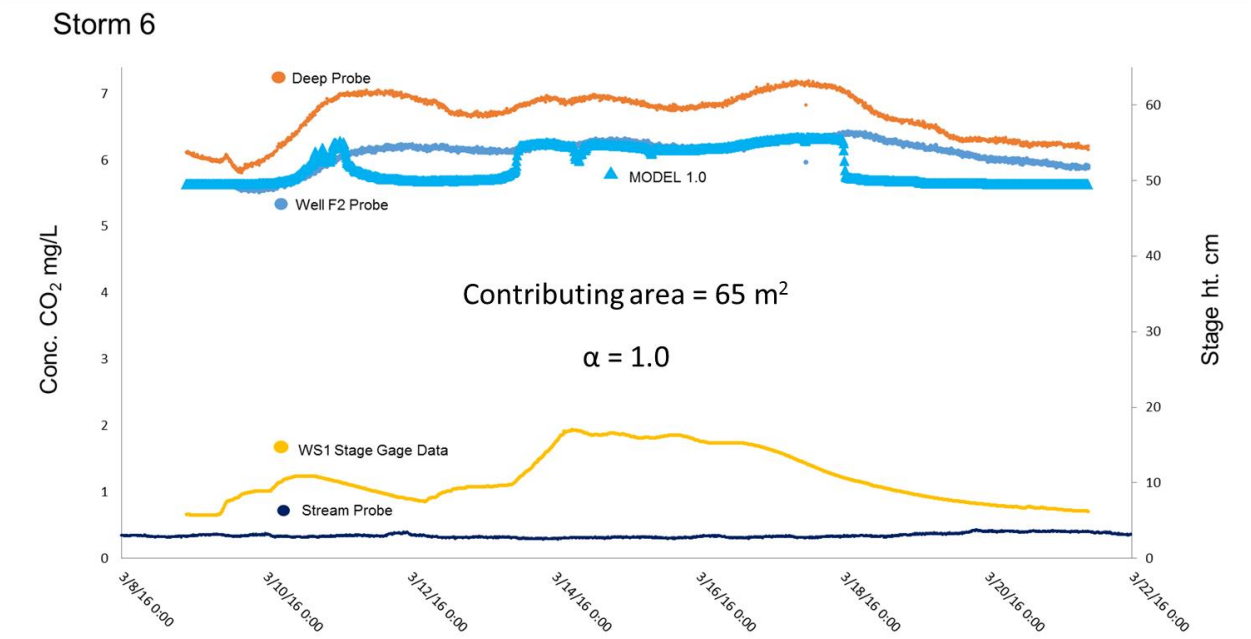

Figure 48. Model response to a change in α. The model is represented by the light blue triangles, the deep probe is the orange line, the well F2 line is the blue line, the stream probe is the dark blue line, and the stream stage height is the yellow line. Interestingly, when α was increased to 1.0, the model was activated throughout the duration of the storm. This indicates complete percolation from the vadose zone before, during, and after the storm event.

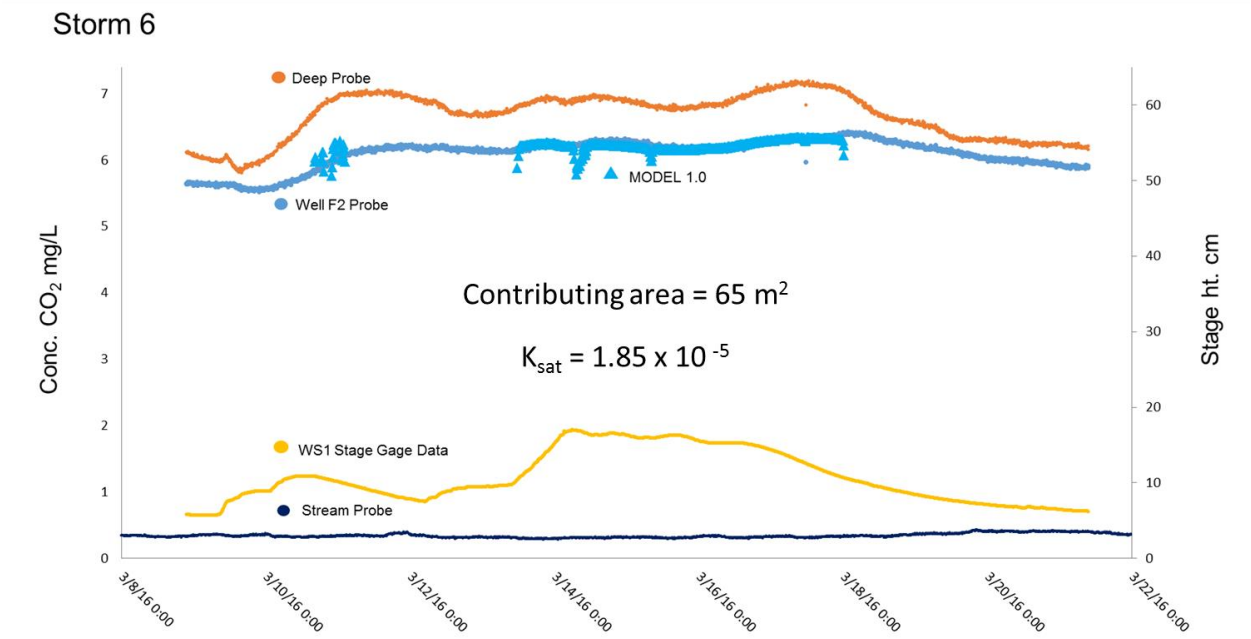

Figure 49. Model results using OSUCAL K_{Sat}. Model results fit observed well F2 CO_2 concentration line.

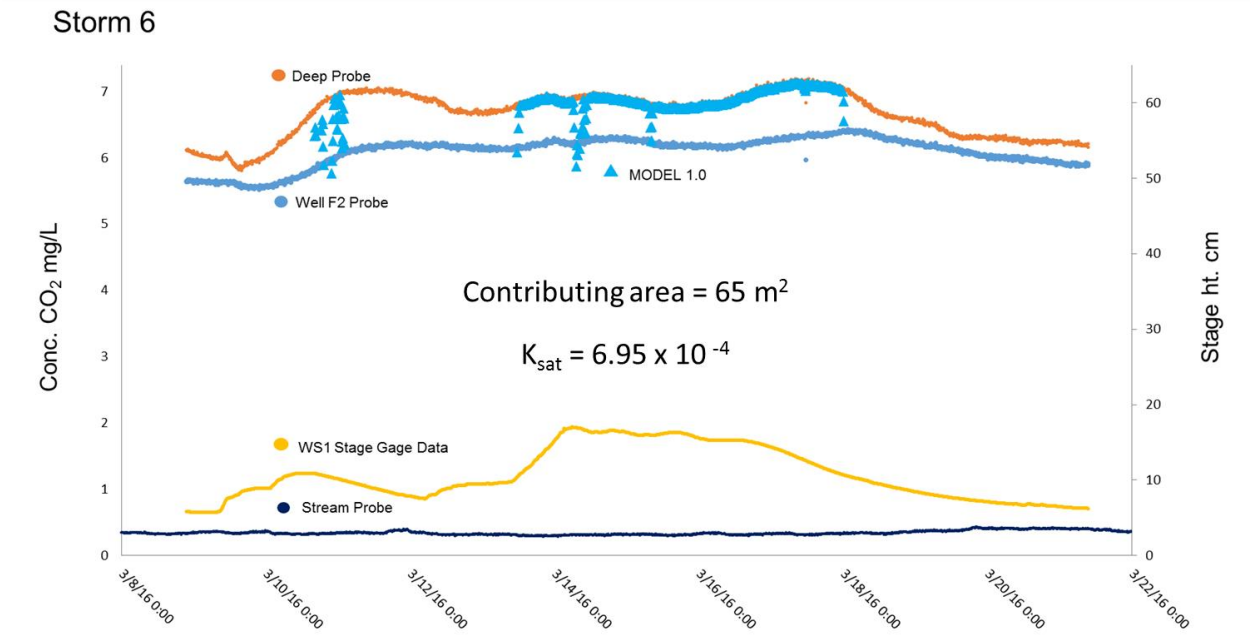

Figure 50. Model results using "Loam" K_{Sat} [*Dingman*, 2008]. Model results fit D CO_2 concentration line at larger K_{sat} value.

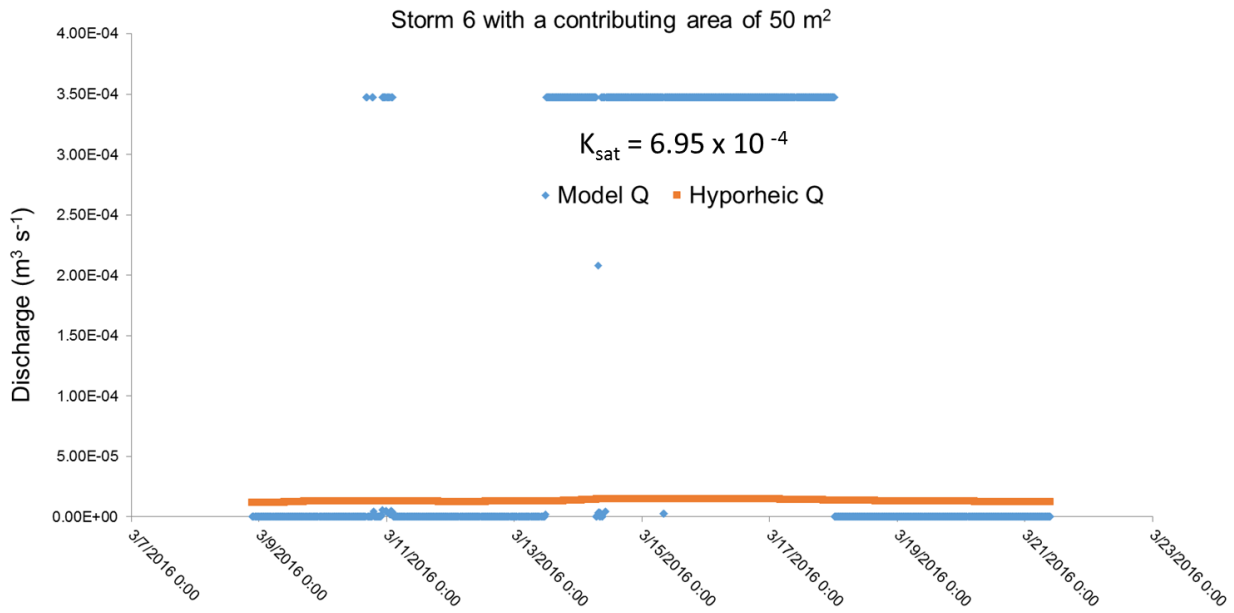

Figure 51. Change in model discharge with K_{sat} increase. The model discharge increases by an order of magnitude with increased K_{sat}.

Parameter	Range of Values					
α	0.0009	0.0001	0.001	0.01	0.1	1

Table 7. α sensitivity analysis range of values.

Parameter	Range of Values						
n	1.0001	1.4	2	4	6	8	10
m	1.0×10^{-4}	0.2857	0.5	0.75	0.8333	0.875	0.9

Table 8. m sensitivity analysis range of values.

Appendix D: Photo Gallery

Figure 52: View of WS1 from above confluence looking northwest.

Figure 53: View of study site from above.

Figure 54: View of well field from bridge.

Figure 55: View of study column.

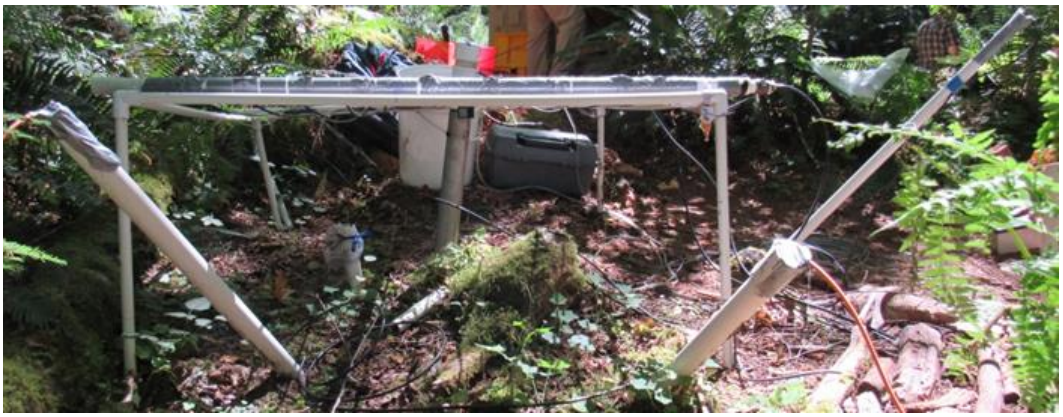

Figure 56: Two additional views of study column and experimental rain simulator.

Figure 57: Vaisala probe in PVC casing.

Figure 58: Deployment of PVC encased probe.

Figure 59: Deployed Vaisala probe in outer PVC casing.

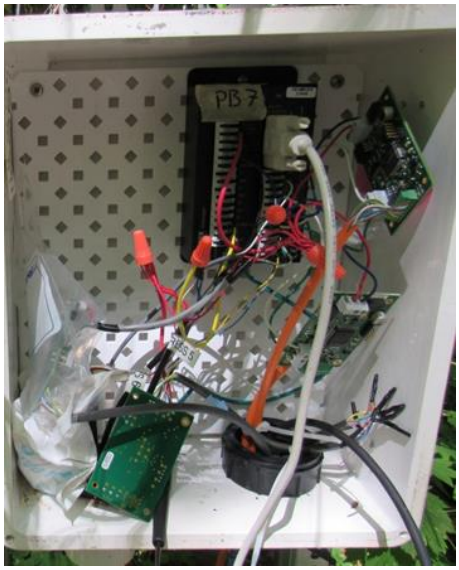

Figure 60: Campbell datalogger.

The following images of the rain collector and the aforementioned rain simulator were part of a rain experiment conducted simultaneously with study column observations. I harvested rain during the previous wet season using the rain collector which was made up of a large Nalgene tank, a tarp and some nets to keep debris out of the tank. I wanted to use rain water as opposed to stream water for our rain simulations because I wanted the water chemistry to be representative of through-fall water. The rain collector was connected to the rain simulator using 1" PVC pipe. The rain simulator was made up of a 1 m2 cage with parallel drip lines fixed at ~6" distances from edge to edge. The pressure for the drip lines was maintained using small valves that can be opened or closed. The pressure was such that drips coming from each hole in the drip lines were of roughly uniform size and timing. I maintained steady pressure during the rain simulations using a small peristaltic pump. I conducted 3 rain simulations at the end of the dry season using ~100 L over a 24 hour period of time. I wanted to try and create the decrease/increase signature in the pCO_2 data observed by *Dosch* [2014]. Additionally, I included a salt tracer in the collected rainwater in order to observe any electrical conductivity activity that may occur in well F2. The purpose of this was to identify when the rain pulse entered the hyporheic zone. There were no significant results or observations with any of the 3 experiments.

Figure 61: View of rain collector from study column.

Figure 62: View of rain collector from trail.

Figure 63: Rain collector close-up.